UCSF

Title

Cross-family small GTPase ubiquitination by the intracellular pathogen Legionella pneumophila

Permalink

https://escholarship.org/uc/item/80n6052x

Journal

Molecular Biology of the Cell, 35(3)

ISSN

1059-1524

Authors

Steinbach, Adriana

Bhadkamkar, Varun

Jimenez-Morales, David

et al.

Publication Date

2024-03-01

DOI

10.1091/mbc.e23-06-0260

Peer reviewed

Cross-family small GTPase ubiquitination by the intracellular pathogen *Legionella pneumophila*

Adriana Steinbach[a,b,†], Varun Bhadkamkar[a,b,†], David Jimenez-Morales[c,d,e], Erica Stevenson[c,d,f], Gwendolyn M. Jang[c,d,f], Nevan J. Krogan[c,d,f], Danielle L. Swaney[c,d,f], and Shaeri Mukherjee[a,b,g,*]

[a]Department of Microbiology and Immunology, and [b]George Williams Hooper Foundation, University of California, San Francisco, CA 94143; [c]Gladstone Institute of Data Science and Biotechnology, J. David Gladstone Institutes, San Francisco, CA 94158; [d]Department of Cellular and Molecular Pharmacology, and [f]Quantitative Biosciences Institute, University of California, San Francisco, CA 94158; [e]Department of Medicine, Division of Cardiovascular Medicine, Stanford University, CA 94309; [g]Chan Zuckerberg Biohub, San Francisco, CA 94158

ABSTRACT The intracellular bacterial pathogen *Legionella pneumophila* (*L.p.*) manipulates eukaryotic host ubiquitination machinery to form its replicative vacuole. While nearly 10% of *L.p.*'s ~330 secreted effector proteins are ubiquitin ligases or deubiquitinases, a comprehensive measure of temporally resolved changes in the endogenous host ubiquitinome during infection has not been undertaken. To elucidate how *L.p.* hijacks host cell ubiquitin signaling, we generated a proteome-wide analysis of changes in protein ubiquitination during infection. We discover that *L.p.* infection increases ubiquitination of host regulators of subcellular trafficking and membrane dynamics, most notably ~40% of mammalian Ras superfamily small GTPases. We determine that these small GTPases undergo nondegradative ubiquitination at the *Legionella*-containing vacuole (LCV) membrane. Finally, we find that the bacterial effectors SidC/SdcA play a central role in cross-family small GTPase ubiquitination, and that these effectors function upstream of SidE family ligases in the polyubiquitination and retention of GTPases in the LCV membrane. This work highlights the extensive reconfiguration of host ubiquitin signaling by bacterial effectors during infection and establishes simultaneous ubiquitination of small GTPases across the Ras superfamily as a novel consequence of *L.p.* infection. Our findings position *L.p.* as a tool to better understand how small GTPases can be regulated by ubiquitination in uninfected contexts.

SIGNIFICANCE STATEMENT

- *Legionella pneumophila* manipulates the host ubiquitin system to form its replicative vacuole, although little is known about which host proteins are differentially ubiquitinated during infection.

- Unbiased mass spectrometry reveals that Legionella targets ~40% of small GTPases in the Ras superfamily with nondegradative mono- and polyubiquitination. Ubiquitination is spatially restricted to GTPases at the replicative vacuole membrane and requires bacterial proteins SidC/SdcA.

- SidE family bacterial proteins subsequently polyubiquitinate Rabs, resulting in retention at the vacuole. Simultaneous GTPase ubiquitination is a novel consequence of *Legionella* infection, and positions *Legionella* as a tool to study small GTPase regulation by ubiquitination in uninfected contexts.

INTRODUCTION

Legionella pneumophila (*L.p.*) is an intracellular bacterial pathogen that has proved to be a master manipulator of its eukaryotic hosts. It is the causative agent of Legionnaires' disease, a severe pneumonia that affects immunocompromised patients upon exposure to contaminated aerosols. In the context of human disease, *L.p.* infects alveolar macrophages, but its preferred hosts include a wide range of protozoa, demonstrating the bacterium's ability to manipulate conserved eukaryotic processes to promote pathogenesis (Best and Kwaik, 2018; Gomez-Valero and Buchrieser, 2019). Phagocytosis by a permissive host cell triggers a complex pathogenic program in which *L.p.* avoids clearance by the endolysosomal system and instead remodels its plasma membrane–derived phagosome into an endoplasmic reticulum (ER)-like compartment called the *Legionella*-containing vacuole (LCV) (Hubber and Roy, 2010). Pathogenesis is mediated by an enormous arsenal of more than 330 bacterial proteins ("effectors") injected into the host cell cytosol by *L.p.*'s Dot/Icm type IV secretion system (T4SS). Characterization of effector function has revealed numerous host targets, including membrane trafficking, autophagy, translation, and protein homeostasis (Qiu and Luo, 2017; Lockwood *et al.*, 2022). Despite these advances, many aspects of *L.p.*-mediated pathogenesis remain elusive, including the functions and targets of most effectors. Studying the effects of these proteins on host cell pathways offers a great potential for the discovery of novel pathogenic and cell biological mechanisms.

Among the many host cell proteins targeted by *L.p.*, small GTPases in the Ras superfamily have long been of interest. Small GTPases are found across eukaryotes, and subfamily members regulate essential cellular functions such as cell proliferation (Ras), intracellular membrane traffic (Rab, Arf), cytoskeletal structure (Rho, Rac), and nuclear import/export (Ran) (Cherfils and Zeghouf, 2013). Despite having disparate cellular functions, these proteins share a similar bimodal activity cycle: an active, membrane-associated, GTP-bound state that allows for the interaction with GTPase-specific binding partners, and an inactive, cytosolic, GDP-bound state. The small GTPase activity cycle is highly regulated—GDP release is mediated by guanine nucleotide exchange factors (GEFs), and GTPase activity and subsequent inactivation is stimulated by GTPase activating proteins (GAPs) (Cherfils and Zeghouf, 2013). GTPase activity, membrane association, and binding interactions can be further regulated by posttranslational modifications (PTMs), providing an additional layer of modular control (Homma *et al.*, 2021; Lei *et al.*, 2021; Osaka *et al.*, 2021). Given the essential roles small GTPases play in the eukaryotic cell and the diversity of regulatory mechanisms used to control GTPase function, pathogens often target GTPases through direct binding interactions and posttranslational modifications (Aktories and Schmidt, 2014), and *L.p.* is no exception. The activity of small GTPases in the early secretory pathway, including Arf1, Sar1, and Rab1, has long been associated with formation of the LCV (Kagan and Roy, 2002; Derré and Isberg, 2004; Kagan *et al.*, 2004). In addition, numerous effectors have been characterized with the ability to bind or posttranslationally modify various small GTPases, as well as recruit or remove small GTPases from the LCV membrane (Nagai *et al.*, 2002; Machner and Isberg, 2006; Murata *et al.*, 2006; Ingmundson *et al.*, 2007; Müller *et al.*, 2010; Mukherjee *et al.*, 2011; Schoebel *et al.*, 2011; Kawabata *et al.*, 2021). Developing an understanding of how small GTPases are regulated during *L.p.* infection has informed a broader understanding of GTPase membrane targeting determinants as well as GTPase regulation via PTMs (Goody *et al.*, 2017), positioning *L.p.* well as a tool to interrogate small GTPase–regulatory mechanisms.

Another central element of *L.p.* pathogenesis is the manipulation of host cell ubiquitin signaling (Luo *et al.*, 2021). Ubiquitin is a small, highly conserved, globular protein used as a PTM to regulate a multitude of eukaryotic cellular processes, including protein degradation/turnover, cell cycle, innate immune signaling, and endocytosis (Komander and Rape, 2012; Yau and Rape, 2016). Ubiquitin is covalently attached to substrate protein lysines using ATP and the sequential activity of ubiquitin-activating (E1), ubiquitin-conjugating (E2), and ubiquitin ligase (E3) enzymes, and can be removed by deubiquitinating enzymes (DUBs). Lysines can be modified with a single ubiquitin (monoubiquitination) or with polymeric ubiquitin chains (polyubiquitination), resulting in a vast array of regulatory outcomes depending on the site of ubiquitination, the ubiquitin chain length, and the linkage pattern of the ubiquitin chain that is formed (Komander and Rape, 2012).

Almost 30 translocated *L.p.* effectors have been characterized to possess either ubiquitin ligase or deubiquitinase activity – a remarkable fact considering that ubiquitin is a eukaryotic protein (Luo *et al.*, 2021). These include the paralogous ligases SidC and SdcA, which promote the recruitment of as yet unknown ubiquitinated substrates and ER membranes to the LCV (Luo and Isberg, 2004; Ragaz *et al.*, 2008; Hsu *et al.*, 2014). SidC/SdcA also play a role in the ubiquitination of two small GTPases important for *L.p.* pathogenesis, Rab1 and Rab10, although how SidC/SdcA are involved and the consequences of ubiquitination on Rab1/10 are not yet known (Horenkamp *et al.*, 2014; Jeng *et al.*, 2019; Liu *et al.*, 2020). The repertoire of secreted ubiquitin ligases also includes the SidE family (SidE, SdeA, SdeB, SdeC), which catalyze noncanonical phosphoribosyl-ubiquitination (PR-ubiquitination), entirely bypassing the host E1-E2-E3 cascade (Bhogaraju *et al.*, 2016; Qiu *et al.*, 2016). A growing list of *L.p.* DUB effectors includes LotC/Lem27, which may regulate the deubiquitination and recruitment of Rab10 (Liu *et al.*, 2020). The tight relationship between *L.p.* pathogenesis and ubiquitin has been further demonstrated by studies connecting host ubiquitin pathways to efficient translocation of effectors through the Dot/Icm T4SS (Ong *et al.*, 2021), ubiquitin binding to the activation of the effector VpdC involved in vacuolar expansion (Li *et al.*, 2022), and effector secretion to the suppression of ubiquitin-rich DALIS structures involved in antigen presentation by immune cells (Ivanov and Roy, 2009).

Thus far, one study has attempted to develop a global understanding of changes in the host ubiquitinome during infection using a proteomic approach. This study revealed that *L.p.* utilizes the ubiquitin-proteasome system to downregulate innate immunity pathways and mTOR signaling during infection (Ivanov and Roy, 2013). However, the proteomic approach used relied on stable cell lines expressing tagged ubiquitin, which are prone to nonspecific ubiquitination (Emmerich and Cohen, 2015; Peng *et al.*, 2017). Modern ubiquitinomics approaches instead rely upon diGlycine (diGly) enrichment, which can be used to detect endogenous ubiquitination events in the absence of tagged ubiquitin overexpression (Xu *et al.*, 2010; Mertins *et al.*, 2013). This technique has been used to perform global analyses of host cell ubiquitinome changes during *Salmonella typhimurium* and *Mycobacterium tuberculosis* infections (Fiskin *et al.*, 2016; Budzik *et al.*, 2020), but has not yet been used for *L.p.*-infected cells. In addition, because distinct subsets of effectors function during early and late stages of *L.p.* infection (Oliva *et al.*, 2018), a dynamic, temporal profile of host protein ubiquitination changes is needed to more deeply understand the regulatory mechanisms at play during infection. We set out to provide an unbiased global analysis of ubiquitin dynamics during *L.p.* infection,

identifying key proteins and processes targeted during *L.p.* infection for ubiquitination and deubiquitination.

To identify proteins with changing ubiquitination status across the span of *L.p.* infection, we undertook a proteome-wide analysis of protein ubiquitination at 1 and 8 h postinfection (hpi) using diGly enrichment and mass spectrometry. Additionally, we quantified protein abundance for the preenriched samples as quality control, and to identify potential degradative versus nondegradative signaling ubiquitination. Strikingly, we discovered that at least 63 of ~160 mammalian small GTPases across all subfamilies are ubiquitinated, but not degraded, during infection in a process dependent upon bacterial effector secretion. Importantly, a growing body of work has found that many small GTPases in the Ras superfamily can be regulated via ubiquitination outside of the context of infection, resulting in profound impacts on their activity consequential for human disease (Lei *et al.*, 2021). This suggests that *L.p.* may coopt existing host regulatory mechanisms to control small GTPase function for its own benefit—an exciting prospect, given that the mechanisms and consequences of ubiquitination remain poorly defined for many small GTPases. Additionally, the degree of simultaneous cross-family small GTPase ubiquitination observed in our proteomics is, to our knowledge, unprecedented. We determine that small GTPases are targeted with both mono- and high molecular weight polyubiquitination during *L.p.* infection, and that ubiquitination is likely nondegradative. Using the small GTPases Rab1, Rab5, and Rab10 as test cases, we demonstrate that robust recruitment of these GTPases to the LCV membrane is required for their ubiquitination. We find that effectors SidC and SdcA are necessary for the ubiquitination of Rab5 and GTPases beyond the Rab subfamily, including RhoA and HRas. Intriguingly, SidC/SdcA are also required for Rab5 recruitment to LCV, suggesting a complex interplay between SidC/SdcA activity, small GTPase membrane association, and ubiquitination. Finally, we determine that effectors in the SidE family function downstream of SidC/SdcA to promote Rab1 and Rab5 polyubiquitination, which facilitates their retention in the LCV membrane. Altogether, our data suggest that *L.p.* modulates small GTPases during infection through the concerted activity of several effectors, resulting in prolific, cross-family small GTPase ubiquitination and retention of GTPases at the LCV membrane. Our work positions *L.p.* as a tool to better understand how small GTPases can be regulated by ubiquitination in uninfected contexts.

RESULTS

L.p. infection induces T4SS-dependent ubiquitinome changes in the host cell

To identify host cell components and pathways targeted with ubiquitin during *L.p.* infection, we performed a global proteomics analysis of protein ubiquitination changes in *L.p.*-infected cells. We chose HEK293 cells stably expressing the FcγRIIb receptor (HEK293 FcγR cells), as HEK293 FcγR have been used extensively in previous studies of *L.p.* pathogenesis and efficiently internalize antibody-opsonized *L.p.* (Mukherjee *et al.*, 2011; Treacy-Abarca and Mukherjee, 2015; Qiu *et al.*, 2016; Black *et al.*, 2019; Moss *et al.*, 2019). Cells were left uninfected or infected with either wild-type (WT) *L.p.* or the nonpathogenic *L.p.* Δ*dotA* strain (Figure 1A). For temporal resolution, infected cells were lysed at 1 or 8 h hpi. Extracted proteins from these five conditions (uninfected control, WT 1 h, WT 8 h, Δ*dotA* 1 h, Δ*dotA* 8 h) were trypsinized and processed with diGly remnant enrichment, which is found upon protein modification with ubiquitin. While diGly enrichment also captures peptides modified with the ubiquitin-like proteins NEDD8 and ISG15, these peptides make up only a small fraction of the total enriched pool (~5%) (Kim *et al.*,

2011). It is important to note that this enrichment strategy can identify only canonically ubiquitinated sites; PR-ubiquitination mediated by the SidE family will not be detected. Enriched peptides were then subjected to mass spectrometric analysis and quantified with appropriate adjustments made based on quality control metrics (see Materials and Methods; Supplemental Table S1; Supplemental Figure S1, A and B). Peptide intensities between all three biological replicates per condition showed a robust reproducibility with correlation coefficients ranging from 0.80 to 0.91 (Supplemental Figure S1C). To capture the overall similarities and differences between the five experimental conditions, we performed a Principal Component Analysis (PCA). PCA identified a larger correlation between uninfected control and Δ*dotA* relative to WT (Supplemental Figure S1D). This indicates that, as expected, most changes in the ubiquitinome during infection are driven by effector secretion from *L.p.* WT.

We next determined how ubiquitination was changing for individual proteins between the different conditions. We calculated the Log2 fold changes (Log2FC), corresponding p values, and adjusted p values for all detected proteins across all pairwise combinations of conditions (uninfected, WT and Δ*dotA* infected). Unsurprisingly, we encountered many instances in which a peptide was uniquely detected in one of the conditions while missed in the other one (e.g., a novel protein ubiquitination detected in WT infected but not uninfected control cells). Log2FC and adjusted p values were calculated for these events using a suitable imputation strategy in which the missing peptide intensity value was assigned from the threshold of detection (see *Materials and Methods*). The full dataset for changes in protein ubiquitination, as well as a dataset containing changes at specific diGly sites (ubiquitin sites tab) can be found in Supplemental Table S2. In our subsequent analyses, we focused on four comparisons: WT1h-Control, WT8h-Control, Δ*dotA*1h-Control, and Δ*dotA*8hr-Control (hereafter referred to as WT1h, WT8h, Δ*dotA*1h, and Δ*dotA*8h). Significant ubiquitination was determined using joint thresholds of |Log2FC| ≥ 1, adjusted p value < 0.05.

Using these significance criteria, we analyzed changes in host protein ubiquitination during WT and Δ*dotA* infections. In accordance with the strong WT *L.p.*-induced ubiquitination signature shown by our PCA, we detected hundreds of proteins with significant ubiquitination changes during WT *L.p.* infection, in stark contrast to the few changes induced during Δ*dotA* infection (Figure 1B). The number of ubiquitinated proteins was highest early in WT *L.p.* infection, with 420 proteins ubiquitinated at 1 hpi and 271 at 8 hpi. In addition, we note that 80% (217 of 271) proteins ubiquitinated at 8 hpi were also ubiquitinated at 1 hpi, demonstrating a high degree of overlapping ubiquitination at early and late timepoints (Figure 1C). Analysis of total ubiquitinated proteins during infection by Western blotting confirms our proteomic data, showing significantly higher levels of ubiquitinated proteins during WT infection compared with Δ*dotA*, as well as a decrease in ubiquitination at 8 hpi (Figure 1D).

To better understand which subcellular compartments were most targeted with ubiquitination or deubiquitination, we used subcellular localization identifiers from UniProt to tabulate the number of significantly regulated proteins per compartment (Figure 1E). In addition, we performed biological pathway and protein complex enrichment (Figure 1F; Supplemental Table S3). Subcellular localization analysis demonstrated the ubiquitination of hundreds of proteins with cytosolic or cell membrane localization, as well as endosomes, the endoplasmic reticulum, and the Golgi apparatus (Figure 1E). Closer study of the enrichment results reveals increased ubiquitination in pathways supporting secretory and endocytic
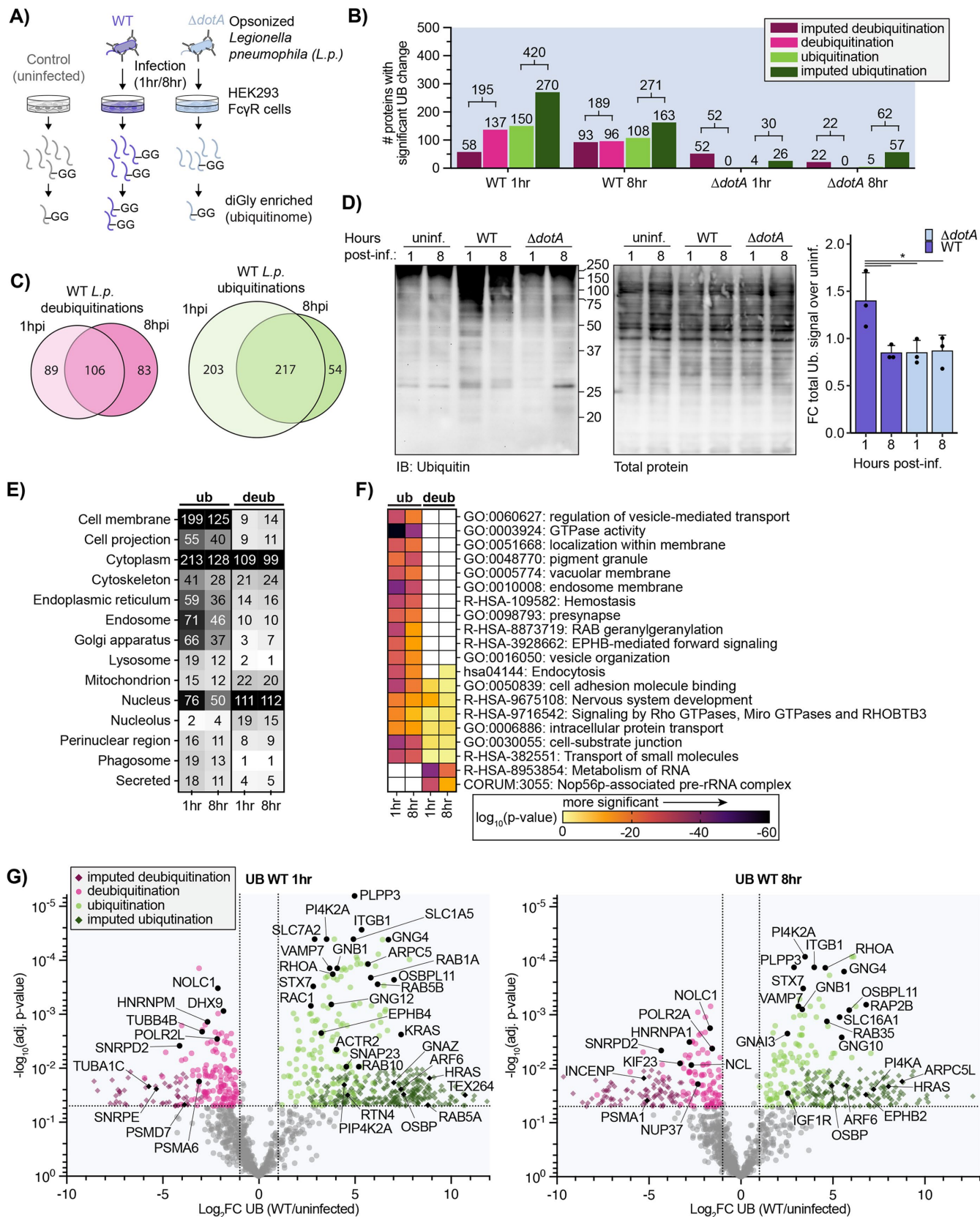
FIGURE 1. *L.p.* infection induces T4SS-dependent ubiquitinome changes in the host cell. (A) Schematic of experimental procedures. (B) Counts of proteins with a significant increase (green) or decrease (magenta) in ubiquitination compared with uninfected control for the indicated infection conditions. (Significance threshold for all subsequent analysis: |log2(FC)|>1, *p*<0.05, see note in text on use of imputation in this dataset). (C) Overlap of proteins with a significant increase (green) or decrease (magenta) in ubiquitination compared with uninfected control in the 1-h vs 8-h WT

membrane trafficking, cytoskeletal dynamics, and membrane biology (Figure 1F). Several of the most strongly enriched terms related to small GTPases and GTPase activity, namely "GTPase activity" and "RAB geranylgeranylation." Further analysis of ubiquitinated proteins revealed proteins in almost all subfamilies of the Ras superfamily of small GTPases, including RAB, RAS, RHO/RAC, RAN, ARF/SAR GTPases (Figure 1G; Supplemental Table S2). While *L.p.* effectors are known to manipulate several of these small GTPases during infection, including Arf1, Rap1, Rab1, Rab10, Rab33b, and Ran (Nagai *et al.*, 2002; Rothmeier *et al.*, 2013; Qiu *et al.*, 2016; Schmölders *et al.*, 2017; Steiner *et al.*, 2018; Jeng *et al.*, 2019; Liu *et al.*, 2020), the targeting of numerous small GTPases with ubiquitination is unprecedented. Regulatory small GTPase ubiquitination is known to occur in uninfected contexts (Lei *et al.*, 2021), suggesting possible widespread manipulation of small GTPase signaling during *L.p.* infection. GTPase ubiquitination during WT infection extended to numerous heterotrimeric G proteins (Figure 1G). This included alpha (GNA11/13/I1/I2/I3/O1/Q/Z), beta (GNB1/2/4), and gamma (GNG4/5/7/10/12) subunits, as well as several regulators of heterotrimeric G protein signaling (RGS17/19/20). Although the role of heterotrimeric G protein signaling has not been studied extensively in the context of *L.p.* infection, it is known that G proteins are important for phagocytosis of *L.p.* in amoeba (Fajardo *et al.*, 2004) and that multiple G proteins are found on the surface of the LCV in proteomic datasets (Hoffmann *et al.*, 2014). Ubiquitination of heterotrimeric G protein subunits can result in a wide variety of signaling outcomes (Dewhurst *et al.*, 2015; Torres, 2016; Dohlman and Campbell, 2019), suggesting *L.p.* or the host cell may modify G protein signaling via ubiquitination during infection.

We also detected ubiquitination on other proteins or pathways known to be targeted by *L.p.* effectors but not known to be targeted with ubiquitination. These include numerous regulators of the actin cytoskeleton (ARPC1B/2/5/5L, ACTR2/3, BAIAP2), proteins involved in lipid exchange (OSBP, OSBPL3/8/9/11, PITPNA), lipid kinases (PI4KA, PI4K2A, PIP4K2A), as well as SNARES and membrane fusion regulators (STX3/6/7/10/12, SNAP23/29, VAPA, NAPA, VAMP7). Also ubiquitinated during infection were several proteins known to be modified with noncanonical ubiquitination by the SidE family of *L.p.* effectors – which is not detected by the diGly enrichment technique used here – including the ER-shaping proteins RTN4, FAM134C, and TEX264 (Shin *et al.*, 2020). In addition, we identified ubiquitination on protein targets previously unknown to play roles in *L.p.* infection, including solute carrier transporters, tyrosine (EPHB1/2/4, FGFR2, IGF1R) and serine/threonine-protein kinases (LIMK1, PKN2, TNIK, MINK1), and integrins (ITGA3/B1/B1BP1/B3).

In addition to protein ubiquitination, *L.p.* infection induced the deubiquitination of hundreds of proteins at both 1 hpi (195 proteins) and 8 hpi (189 proteins) (Figure 1B). Of these, 106 proteins were deubiquitinated at both timepoints, suggesting that early and late infection deubiquitination is targeted to many of the same proteins (Figure 1C). Unlike the strong ubiquitination of cell membrane proteins, proteins deubiquitinated during WT infection primarily localized to the nucleus and the cytoplasm (Figure 1E). Pathway enrichment analysis of deubiquitinated proteins showed minimal overlap with pathways targeted by ubiquitination, suggesting that protein populations targeted for ubiquitination and deubiquitination during infection are distinct (Figure 1F). In line with a distinct, nuclear-enriched deubiquitination response, enrichment analysis primarily described deubiquitinated proteins with the two terms "Metabolism of RNA" and "Nop56p-associated pre-rRNA complex." These enrichments are driven in part by deubiquitination of numerous spliceosome proteins (HNRNPA1/C/K/M/U, SNRPD2/D3/E, SF3B3/B6), as well as transcription regulators (DHX9, POLR2A/2L) and the multifunctional proteins nucleolin (NCL) and NOLC1 (Figure 1G). Although none of these proteins are known targets of *L.p.* effectors, host cell transcription is known to be modulated by the *L.p.* effectors LegAS4/RomA (Rolando *et al.*, 2013), LphD (Schator *et al.*, 2023), LegA3/AnkH (Dwingelo *et al.*, 2019), and SnpL (Schuelein *et al.*, 2018) through a variety of mechanisms, suggesting that *L.p.* may use additional effectors to target nuclear function. Intriguingly, we also observed the deubiquitination of numerous subunits of the proteasome (PSMA1/A6/B3/C1/C3/C5/D1/D7, ADRM1), which is known to be important for *L.p.* infection (Dorer *et al.*, 2006; Price *et al.*, 2011). We also noticed deubiquitination of several regulators of the RAN GTPase (RANBP2, RCC1) and associated proteins such as nuclear pore complex (NUP37/85/188, TPR), tubulin subunits (TUBA1C, TUBB, TUBB4B), the microtubule stabilizer CKAP2, and microtubule-associated proteins (PCM1, INCENP, KIF23, CEP131). The deubiquitination of these proteins is intriguing because *L.p.* is known to activate the Ran GTPase – promoting microtubule polymerization and LCV motility – with the effectors LegG1 and PpgA (Rothmeier *et al.*, 2013; Simon *et al.*, 2014; Swart *et al.*, 2020). Altogether, *L.p.* induces the deubiquitination of hundreds of proteins over the course of infection on a population distinct from proteins targeted with ubiquitination.

In contrast to WT infection, Δ*dotA* induced few changes in both protein ubiquitination and deubiquitination at both 1 and 8 hpi (Figure 1B; Supplemental Figure S2). The few changes that did occur during Δ*dotA* infection primarily occurred in the nucleus, cytoplasm, and cell membrane (Supplemental Figure S2D), and were described by terms known to relate to bacterial infection such as "Bacterial invasion of epithelial cells", "PID NFkappaB Canonical Pathway", "lytic vacuole," and "PCP/CE pathway" (planar cell polarity pathway) (Supplemental Figure S2E) (Tran *et al.*, 2014). The enrichment of these terms during Δ*dotA* infection indicates a strong

---

L.p.–infected conditions. (D) Immunoblot analysis of the total pool of ubiquitinated proteins in HEK293T FcγR cells infected with WT or Δ*dotA L.p.* (MOI = 20) for 1 or 8 h, or left uninfected. Invitrogen No-Stain protein labeling reagent was used to quantify total protein before immunoblot analysis. Total ubiquitin signal was first normalized to total protein for each sample, then the fold change over the appropriate uninfected sample was calculated (*N* = 3). (E) Subcellular localization analysis of proteins with a significant increase or decrease in ubiquitination compared with uninfected control during WT *L.p.* infection for 1 or 8 h. (F) Pathway and protein complex analysis of proteins with a significant increase or decrease in ubiquitination compared with uninfected control during WT *L.p.* infection for 1 or 8 h. Terms not significantly enriched for a given experimental condition are represented by white boxes. Analysis performed using Metascape (see *Materials and Methods*). (G) Volcano plot representation of all ubiquitinome data in WT vs uninfected comparison at 1 and 8 h postinfection. Imputed values are shown as diamonds. Significance threshold is indicated by the dotted line.

antibacterial host response that is absent during WT *L.p.* infection and serves as a confirmation that our proteomic analysis aligns with the biology of the system.

Given the tight relationship between protein ubiquitination and degradation, we compared host cell protein ubiquitin changes to changes in abundance. To do this, we analyzed our pre-diGly–enriched cell lysates via mass spectrometry and quantified changes in host protein abundance. As with our ubiquitinomics, peptide intensities showed robust reproducibility and PCA distinctly separated WT-infected cells from uninfected and Δ*dotA*-infected cells (Supplemental Figure S3). Log2 fold changes, corresponding *p* values, and adjusted *p* values for all detected proteins across all pairwise combinations of conditions were computed and analyzed and can be found in Supplemental Table S2 (abundance tab) and Supplemental Figure S4, A–D. To compare protein ubiquitination and abundance changes, we plotted ubiquitination Log2FC values against abundance Log2FC for all detected proteins at 1 and 8 hpi (Supplemental Figure S4E). Again, we used a significance cutoff of |Log2FC| ≥ 1, adjusted *p* value < 0.05 to determine proteins significantly changing in abundance, ubiquitination, or both abundance and ubiquitination. Importantly, few proteins experienced significant changes in both abundance and ubiquitination simultaneously. This result serves as a quality control that changes in abundance are not responsible for detected changes in ubiquitination and suggests that ubiquitination largely does not result in protein abundance changes during infection.

L.p. infection results in the ubiquitination of multiple Ras superfamily small GTPases

Among the many ubiquitin-regulated pathways and proteins during infection, we were particularly intrigued by the ubiquitination of many small GTPases in the RAS superfamily. Previous studies have shown that *L.p.* uses ubiquitin to modify select small GTPases in the Rab subfamily. Two Rab proteins known to play important roles in pathogenesis, Rab1 and Rab10, are ubiquitinated during infection in a process dependent upon the paralogous effectors SidC and SdcA (Kagan *et al.*, 2004; Horenkamp *et al.*, 2014; Jeng *et al.*, 2019). In addition, Rab33b is PR-ubiquitinated by the SidE family of ligases (Qiu *et al.*, 2016). Although the consequences of Rab1/10/33b ubiquitination are not known, both SidC/SdcA and SidE family effectors are associated with timely LCV formation, suggesting small GTPase ubiquitination may be part of a central *L.p.* pathogenesis program. Additionally, although small GTPases are known to be regulated by ubiquitination outside the context of infection, the simultaneous cross-family ubiquitination of these proteins is unprecedented and suggests that *L.p.* may exploit a GTPase regulatory mechanism common to the entire superfamily (Lei *et al.*, 2021). Thus, we further investigated *L.p.*-induced cross-family small GTPase ubiquitination to learn more about *L.p.* pathogenesis, but also GTPase regulation more broadly.

We first identified the number and family range of small GTPases ubiquitinated during infection in our ubiquitin site dataset (Supplemental Table S2, ubiquitin_sites tab). Small GTPases in the Ras superfamily accounted for 132 of 868 significant ubiquitination sites (15.21%) at 1 hpi, and 77 of 532 (14.47%) significant ubiquitination sites at 8 hpi (Figure 2A; Supplemental Figure S5). Ubiquitination sites were detected on at least 63 of the ~163 known mammalian Ras superfamily small GTPases, falling on members of the ARF, RAN, RHO/RAC, RAS, and RAB subfamilies (Supplemental Figure S6). Many of these ubiquitination sites were imputed, suggesting that the ubiquitination of these proteins may result from *L.p.* effector activity (Supplemental Figure S6). While several of the

small GTPases ubiquitinated during infection are known to be regulated by ubiquitin outside of the context of infection, these ubiquitination events are often transient and hard to detect (Lachance *et al.*, 2013; Shin *et al.*, 2017; Sapmaz *et al.*, 2019; Duncan *et al.*, 2022), suggesting that *L.p.* infection may ubiquitinate small GTPases at a higher frequency or with a greater stability than observed in uninfected cells. In contrast to WT infection, Δ*dotA* infection induced ubiquitination of few small GTPases, consistent with cross-family small GTPase ubiquitination being a process induced by secreted effectors.

Because our diGly enrichment ubiquitinomics strategy precludes determination of ubiquitin chain length, we assessed the ubiquitination of multiple Ras superfamily small GTPases via Western blot analysis. We transfected HEK293T FcγR cells with a panel of GFP-tagged or Flag-tagged GTPases and infected them with WT or Δ*dotA* *L.p.* We expected ubiquitinated GTPases to show the appearance of bands in multiples of ~8.5 kDa (molecular weight of a ubiquitin moiety) above the major, nonubiquitinated species. Indeed, numerous GTPases in the ARF (ARF1, ARF6), RAS (HRas, Rap1, Rap2B), RHO (RhoA, RhoB, RhoC, RhoQ), and RAB (Rab6A, Rab9A, Rab20, Rab35) subfamilies showed a prominent mass shift consistent with monoubiquitination during WT but not Δ*dotA* infection (Figure 2, B–E; Supplemental Figure S7). In many circumstances, we noticed multiple mass shifts above the unmodified band, as well as the accumulation of high molecular weight species. These bands are consistent with the conjugation of either extended polyubiquitin chains, or multiple monoubiquitin moieties to distinct lysine residues on these small GTPases (poly-monoubiquitination). The accumulation of both mono- and high molecular weight ubiquitinated species is also consistent with past experimentation on Rab1/10 ubiquitination during infection (Horenkamp *et al.*, 2014; Jeng *et al.*, 2019; Liu *et al.*, 2020). Altogether, our results confirm the cross-family GTPase ubiquitination observed in our mass spectrometric data and suggest that small GTPases are targeted for both mono- and polyubiquitination during infection.

To determine whether cross-family small GTPase ubiquitination may promote degradation, we mined our AB dataset for changes in small GTPase abundance during infection (Figure 2F). Of the many detected GTPases, almost all fell below both the adjusted *p* value and the Log2FC significance cutoffs, suggesting that GTPases do not significantly change in abundance during infection. This result is consistent with past work demonstrating that *L.p.*-induced Rab1 ubiquitination is removed at later time points during infection in a proteasome-independent process (Horenkamp *et al.*, 2014), and with past work on nondegradative small GTPase monoubiquitination (Sapmaz *et al.*, 2019; Kholmanskikh *et al.*, 2022). Consistent with this insight from our proteomics analysis, we do not see a decrease in small GTPase abundance across the time course of infection by Western blot analysis for all small GTPases tested (Figures 2, B–E and 5; Supplemental Figure S7).

We next decided to explore small GTPase sequence and structure for clues regarding the impacts of ubiquitination. Towards this end, we aligned the sequences of the significantly ubiquitinated GTPases, annotated regions of interest, and marked all unique ubiquitination or deubiquitination sites from both 1 and 8 hpi (Supplemental Figure S8 – full alignment; Figure 3A – Rab1A only). Regions of interest include: 1) the five conserved G boxes important for contact with GTP/GDP; 2) the Switch I and Switch II regions important for interaction between active GTPases and their downstream binding partners; 3) the C-terminal hypervariable domain (HVD) typically responsible for proper membrane targeting and
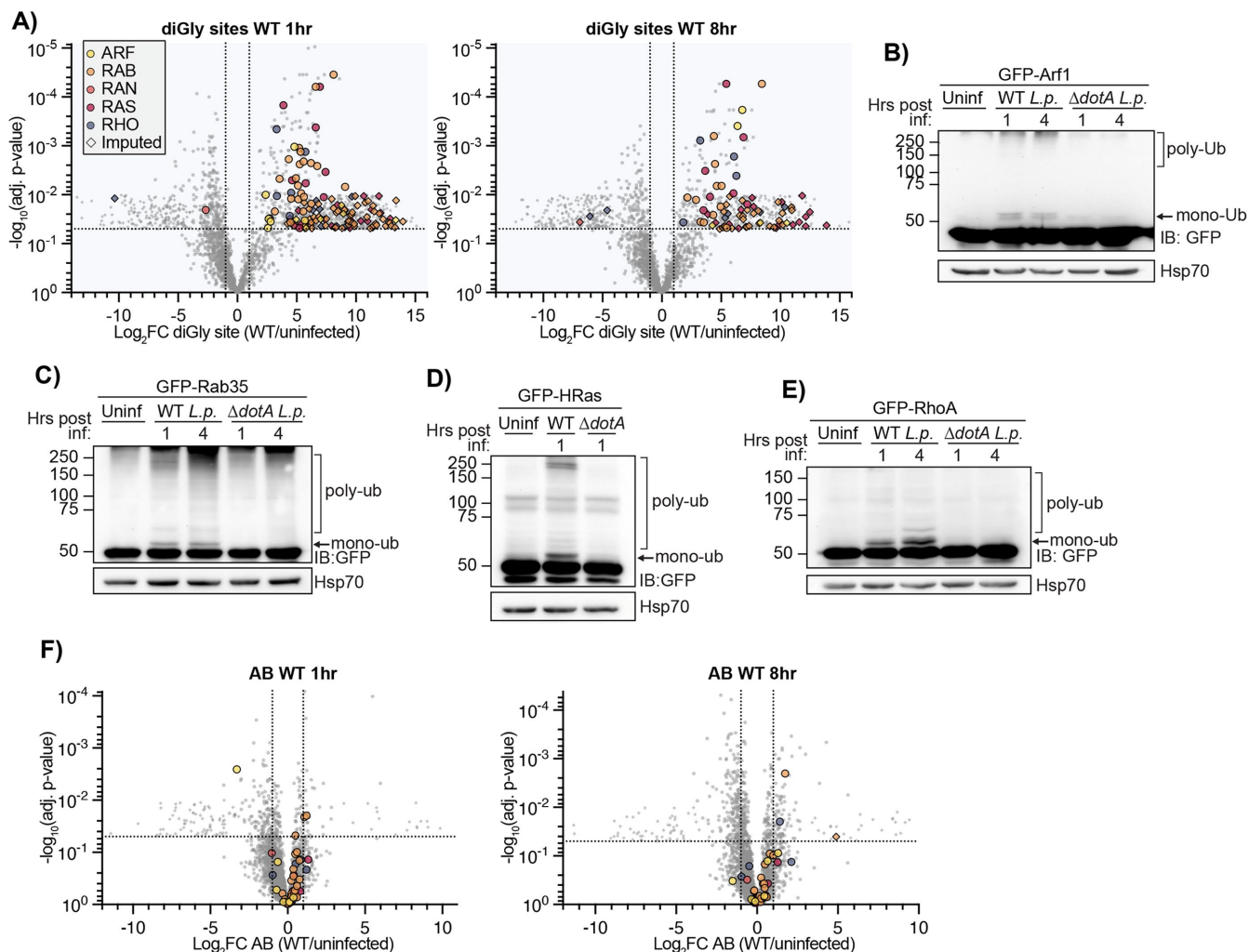
FIGURE 2. Small GTPases across the Ras superfamily are ubiquitinated during WT *L.p.* infection. (A) Volcano plot representation of diGly site dataset for WT *L.p.* versus uninfected comparison at 1 and 8 h postinfection. Each point represents a unique diGly enriched peptide; for some GTPases, multiple peptides were detected. Imputed values are shown as diamonds, and Ras superfamily subfamilies are differentiated by color. Significance threshold is shown by the dotted line. (B–E) Immunoblot analysis of lysates prepared from HEK293T FcγR cells transiently transfected with the indicated GFP-tagged small GTPase, then infected with either WT or Δ*dotA L.p.* (MOI = 50) for 1 or 4 h, or left uninfected. Blots were probed with anti-GFP and anti-Hsp70 antibodies. (F) Volcano plot representation of abundance dataset as in (A).

subcellular localization; and 4) the five alpha helices and six beta sheets characteristic of most Ras superfamily small GTPases. We next defined 10 regions based on these conserved structural and functional elements. Within each region, we counted the number of WT *L.p.*-induced ubiquitin sites (Figure 3B). Surprisingly, most of the ubiquitination did not occur in Switch I/II regions (regions #3 and #5), known to be targeted with PTMs by many pathogens (including *L.p.*) to block interaction between active GTPases and their downstream binding partners (Aktories and Schmidt, 2014). Instead, 92 of 138 unique ubiquitination sites (~67%) were detected within the three C-terminal regions: the α4 helix (region #8, 35 sites), G5 box lysine (region #9, 21 sites), and α5/C-terminal hypervariable domain (region #10, 36 sites) (Figure 3B). Intriguingly, most work on small GTPase ubiquitination in uninfected contexts has determined ubiquitination to primarily fall within these regions (Steklov *et al.*, 2018; Osaka *et al.*, 2021; Kholmanskikh *et al.*, 2022), suggesting that *L.p.* infection hijacks GTPase-regulatory regions also targeted in the absence of infection.

We next mapped ubiquitinated regions onto the structure of the small GTPase Rab1 (Figure 3C, pink regions). To visualize the relationship between these ubiquitinated regions, key functional regions, and protein-binding interfaces, we also aligned the structure of Rab1 to structures of GTPases bound to several types of partners, including Rab1 bound to the *L.p.* secreted Rab-binding effector LidA, yeast YPT1 (Rab1 homologue) bound to GDI, and mouse Rab6 bound to Rab6-interacting protein 1 (R6IP1) (Figure 3D). As expected, LidA, GDI, and R6IP1 predominantly form contacts with GTPases around the Switch I/II regions. To our surprise, the dominantly ubiquitinated regions #8, #9, and #10, localize to the distal face of Rab1, opposite protein-binding regions. This result implies that cross-family small GTPase ubiquitination may not directly block GTPase-protein–binding interactions, and instead, affect other intrinsic GTPase properties, such as membrane association, GTP/GDP binding, or GTP hydrolysis, or may affect protein-binding interactions through an allosteric mechanism.
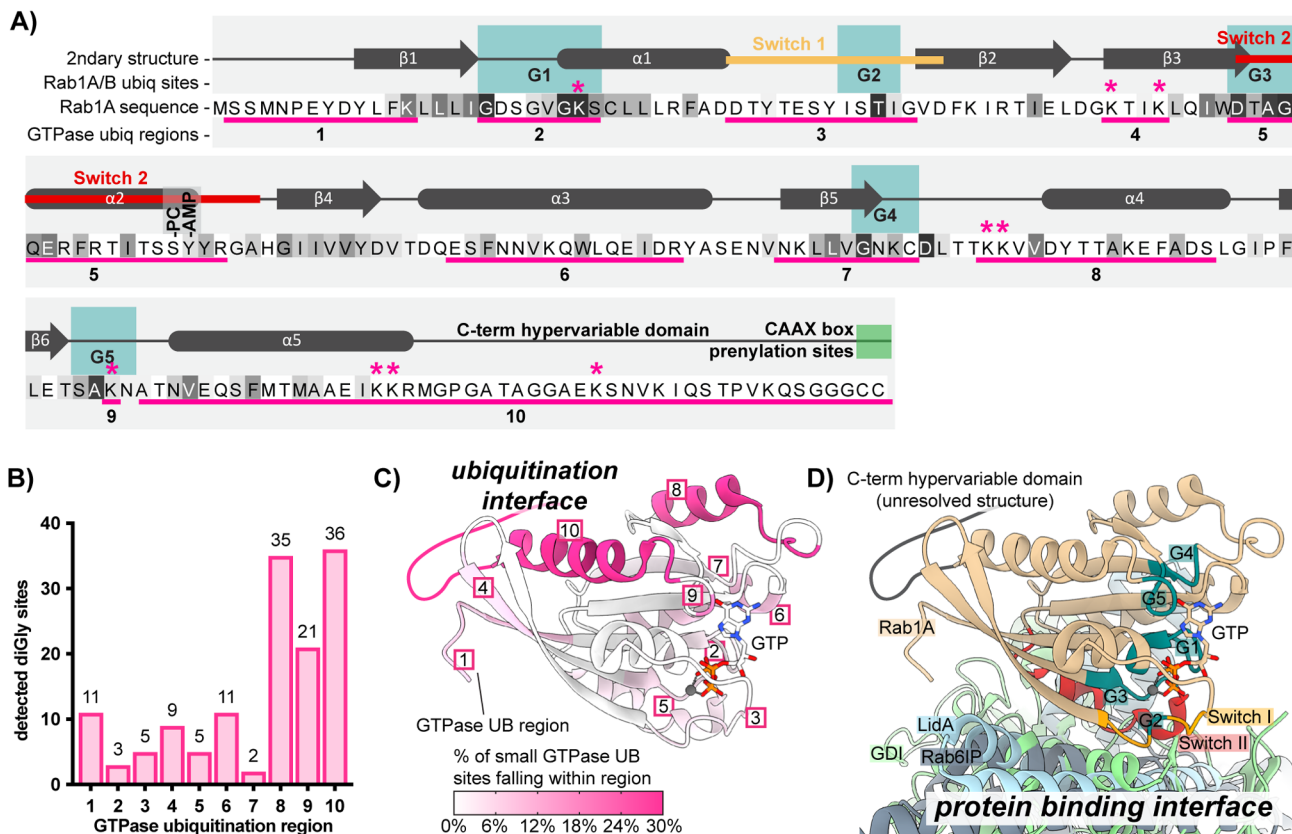
FIGURE 3. Small GTPase ubiquitinations cluster in the C-terminal region. (A) Schematic of small GTPase structural and functional regions, using Rab1A as an example. Regions frequently ubiquitinated across detected small GTPases are underlined in pink and numbered 1–10. Sequence colored by conservation within the small GTPase superfamily, from white (nonconserved) to black (extremely highly conserved residue); see full alignment in Figure 3S1. The "*" symbol indicates ubiquitination sites detected for Rab1A or Rab1B. The site of phosphocholination by *L.p.* effector AnkX (S79) is annotated as "-PC", while the site of AMPylation by *L.p.* effector DrrA (Y80) is marked as "-AMP." (B) Pooled counts of significant ubiquitinations detected in ubiquitination regions defined in (A) across all 63 ubiquitinated small GTPases. (C) Structure of Rab1A with the 10 structural/functional regions indicated. Regions are colored by percentage of detected small GTPase ubiquitin sites falling within a given region. (D) Alignment of structures for human Rab1A (tan) in complex with *L.p.* effector LidA (light blue), mouse Rab6 bound to its effector Rab6IP (gray), or yeast Rab1 homologue YPT1 bound to GDI (light green). Important structural and functional domains of Rab1A are colored and labeled. PDB accession numbers: 3TKL (Rab1A:LidA), 2BCG (YPT1:GDI), and 3CWZ (Rab6:R6IP1).

LCV-localized pools of Rab1 are targeted for ubiquitination

We next interrogated the driving forces behind small GTPase ubiquitination during infection more directly. Based on previous studies, we hypothesized that small GTPase ubiquitination may be spatially restricted to LCV membrane–localized pools of these proteins. First, past work on Rab1 has shown its ubiquitination at 1 hpi and deubiquitination by 8 hpi, which correlates with Rab1 LCV recruitment and removal (Kagan *et al.*, 2004; Ingmundson *et al.*, 2007; Horenkamp *et al.*, 2014). Second, the effectors SidC/SdcA are known to control both Rab10 LCV recruitment and ubiquitination, suggesting a functional link between these two processes (Jeng *et al.*, 2019; Liu *et al.*, 2020). Finally, it is well established that the LCV accumulates ubiquitinated proteins throughout the first 6 to 8 h of infection, indicating that the LCV membrane may be a site of ubiquitin ligase activity (Dorer *et al.*, 2006; Ivanov and Roy, 2009).

To test our hypothesis, we manipulated the recruitment of Rab1 to the LCV during infection and assessed changes in Rab1 ubiquitination. Recruitment of Rab1 was manipulated by altering the activity of the *L.p.* effector DrrA (also known as SidM), which recruits Rab1 to the LCV at early timepoints during infection via the activity of a

Rab1-specific GEF domain and retains Rab1 in the LCV membrane via the activity of its AMP-transferase, or AMPylation domain (Murata *et al.*, 2006; Müller *et al.*, 2010; Hardiman and Roy, 2014). Past work has demonstrated that a DrrA genomic deletion *L.p.* strain ΔdrrA displays considerably reduced Rab1 recruitment to the LCV, and that DrrA AMPylation activity is required, as complementation with AMPylation-dead DrrA D110,112A fails to rescue Rab1 recruitment (Hardiman and Roy, 2014). Consistent with Rab1 LCV recruitment and retention being tied to its ubiquitination, we found considerably reduced levels of Rab1 mono- and polyubiquitination during infection with *L.p.* ΔdrrA and *L.p.* ΔdrrA + pDrrA D110,112A compared with *L.p.* WT (Figure 4, A and B, quantified as % change in normalized Rab1 monoubiquitination). Ubiquitination was rescued by complementation of *L.p.* ΔdrrA with a plasmid expressing WT DrrA. In contrast, DrrA knockout and AMPylation-mutant strains had no effect on the ubiquitination of Rab10, suggesting that DrrA does not control the ubiquitination of GTPases not targeted by its GEF domain (Supplemental Figure S9, A and B).

To further interrogate the relationship between Rab1 recruitment to the LCV membrane and its ubiquitination, we sought to prevent
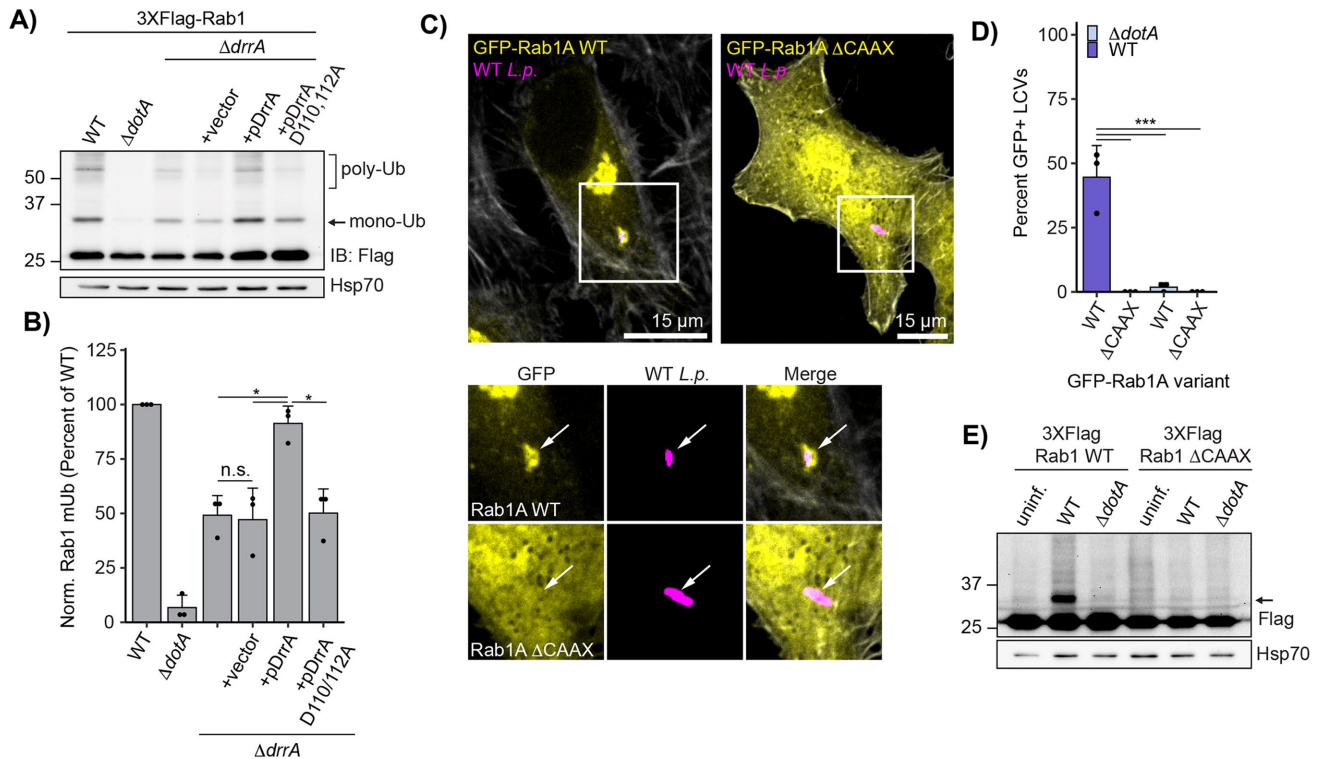
FIGURE 4. Rab1A is monoubiquitinated at the LCV membrane. (A) Immunoblot analysis of lysates prepared from HEK293T FcγR transfected with 3XFlag Rab1A and infected with a Δ*drrA L.p.* strain panel (WT, Δ*dotA*, Δ*drrA*, and Δ*drrA* complemented with empty vector or plasmid encoded DrrA WT or D110, 112A) for 1 h (MOI = 50). Monoubiquitinated Rab1 indicated with an arrow. (B) Quantification of biological replicates (*N* = 3) of experiment shown in (A). Normalized Rab1A monoubiquitination intensity was calculated as a percentage of WT *L.p.* infection levels (see *Materials and Methods*). (C and D) Immunofluorescence analysis of EGFP Rab1A WT or ΔCAAX LCV recruitment. HeLa FcγR cells were transfected with indicated construct, then infected for 1 h with either WT or Δ*dotA L.p.* (MOI = 1), fixed, and stained with anti-*Legionella* antibody. (C) Representative images, and (D) quantification of EGFP-positive LCVs (percent of total scored per biological replicate, *N* = 3, 25 LCVs scored/replicate). (E) Immunoblot analysis of monoubiquitination of Rab1A WT vs ΔCAAX during *L.p.* infection. HEK293T FcγR cells were transfected with either 3X Flag Rab1A WT or ΔCAAX, then infected with WT or Δ*dotA L.p.* for 1 h (MOI = 50) or left uninfected. Lysates were probed with anti-Flag antibody. Monoubiquitinated Rab1 indicated with an arrow.

Rab1 association with membranes entirely. To this end, we generated a lipid anchor mutant of Rab1 by deleting its two prenylation sites: the C-terminal cysteines C204 and C205 (known as the CAAX box). As expected, Rab1 ΔCAAX showed fully cytosolic localization compared with the predominantly Golgi-localized WT Rab1 and was not recruited to the LCV membrane (Figure 4, C and D). Consistent with LCV membrane recruitment being a prerequisite for Rab1 ubiquitination, Rab1 ΔCAAX ubiquitination was entirely abolished during infection (Figure 4E). We note a similar loss of ubiquitination upon deletion of the Rab10 CAAX motif (Supplemental Figure S9C). Collectively, our data suggest that only LCV-localized pools of Rab1 are targeted for ubiquitination, and that membrane recruitment may be a prerequisite for infection-induced small GTPase ubiquitination.

Early endosomal GTPase Rab5 is recruited to the LCV and targeted for ubiquitination

We next turned to another small GTPase generally thought to be an antagonist in the *L.p.* infection cycle, Rab5 (Anand *et al.*, 2020). The three genetically encoded Rab5 isoforms (Rab5A, B, and C), particularly Rab5A/B (Chen *et al.*, 2009, 2014), are considered master regulators of the early endosomal compartment, recruiting proteins that direct recently endocytosed cargo within the cell and control endosomal fusion or fission (Langemeyer *et al.*, 2018). Rab5 is required

for endosome maturation, a remodeling of the protein and lipid components of the endosomal membrane that marks the transition from early to late endosome. Unlike early endosomes, late endosomes can fuse with lysosomes, resulting in the degradation of enclosed cargo (Langemeyer *et al.*, 2018). It is well established that WT *L.p.* evades lysosomal fusion, whereas Δ*dotA L.p.* succumbs to lysosomal degradation, suggesting that bacterial effectors prevent endosome maturation at the LCV membrane (Roy *et al.*, 1998; Clemens *et al.*, 2000b). As such, Rab5 has been a protein of interest in the study of *L.p.* pathogenesis for years. Several bacterial effectors have been proposed to be activated by Rab5 binding (Gaspar and Machner, 2014) or regulate Rab5 activity (Sohn *et al.*, 2015), but to our knowledge, none have been shown to directly posttranslationally modify Rab5.

Increased ubiquitination is detected for all three Rab5 isoforms in our ubiquitinome dataset during WT, but not Δ*dotA*, *L.p.* infection (Supplemental Figure S5 and Table S2). The accumulation of an ~8.5 kDa upshifted species is observed for endogenous Rab5A in U937 macrophage lysates across the first 6 h of WT *L.p.* infection (Figure 5A). Endogenous Rab5A and Flag-tagged Rab5B and C also show this mass shift in WT *L.p.*-infected HEK293T FcγR (Supplemental Figure S10, A–C). To confirm that this higher molecular weight species is monoubiquitinated Rab5A, we immunopurified Flag-Rab5A
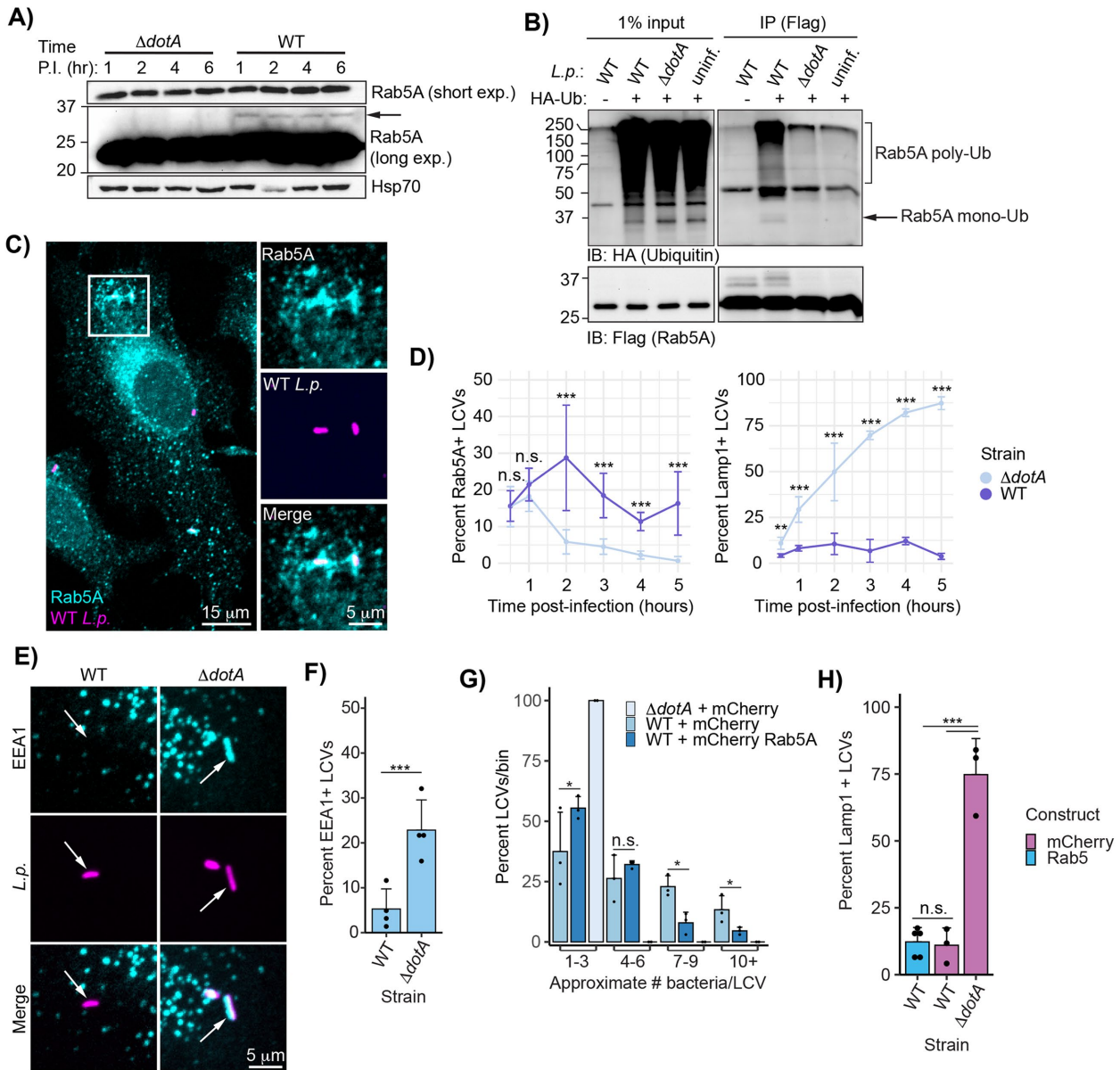
FIGURE 5. Rab5A is recruited to the LCV and ubiquitinated during WT *L.p.* infection. (A) Immunoblot analysis of Rab5A mass shift during WT or Δ*dotA L.p.* infection. U937 cells differentiated into macrophage-like cells were infected with either WT or Δ*dotA* (MOI = 50) and lysed at the indicated time point. (B) Immunoblot analysis of Flag-Rab5A immunoprecipitation from *L.p.*-infected cells. HEK293T FcγR cells transfected with 3XFlag Rab5A and HA-ubiquitin (or vector control) were infected with WT or Δ*dotA* (MOI = 20) for 4 h or left uninfected. After Flag pulldown, input and IP samples were probed with anti-HA and anti-Flag antibodies. (C and D) Immunofluorescence analysis of Rab5A and Lamp1 LCV recruitment. HeLa FcγR cells were infected with WT or Δ*dotA* (MOI = 1) for indicated length of time, fixed, and probed with either anti-Rab5A or anti-Lamp1 antibody. (C) Representative image of WT LCV Rab5A recruitment (1 hpi). (D) quantification of all experiments performed. For each biological replicate, the percent of LCVs scored positive for the indicated marker was calculated (*n* = 3, 75-150 LCVs scored per replicate, Bonferroni adjusted *p* value = 0.08). (E) Rab5 binding partner EEA1 associates with the Δ*dotA* but not WT LCV. HeLa FcγR cells were infected with *L.p.* WT or Δ*dotA* (MOI = 1) for 1 h, fixed, and probed with anti-EEA1 and anti-*Legionella* antibodies. (F) Quantification of biological replicates performed as in (A). For each biological replicate, the percent of LCVs scored positive for the indicated marker was calculated (*n* = 4, 75-150 LCVs scored per replicate, *p* value = 0.05). (G) *L.p.* replication is inhibited by Rab5A overexpression. HeLa FcγR cells were transfected with mCherry tagged Rab5A or mCherry alone, infected with WT or Δ*dotA* for 10 h, fixed, and probed with anti-*Legionella* antibodies. Bacteria count per LCV was approximated by measuring the LCV area and dividing by the average area of the Δ*dotA* LCVs. For each biological replicate (*n* = 3, 25-50 LCVs per replicate, Bonferroni adjusted *p* value = 0.013), the number of LCVs falling into the indicated bin was tabulated, and the percent each bin represented of the total was calculated. (H) Rab5 overexpression does not increase WT LCV Lamp1 staining. HeLa FcγR cells were transfected with mCherry-tagged Rab5A or mCherry alone, infected with WT or Δ*dotA* for 4 h, fixed, and probed with anti-Lamp1 and anti-*Legionella* antibodies. For each biological replicate, the percent of LCVs scored positive for the indicated marker was calculated (*n* = 3–4, 75–150 LCVs scored per replicate, Bonferroni adjusted *p* value = 0.017).

from HEK293T FcγR cells coexpressing low levels of HA-ubiquitin (see *Materials and Methods*) and infected with *L.p.* WT or Δ*dotA*. In WT-infected, but not Δ*dotA*-infected or uninfected pulldown samples, we observe both a discrete band at ~37 kDa when blotting for HA, as well as higher molecular weight species, corresponding to mono- and polyubiquitinated Rab5A, respectively (Figure 5B). Pulldown on endogenous ubiquitin from cells expressing Flag-Rab5A also shows the accumulation of mono- and polyubiquitinated Rab5 in WT-infected cells (Supplemental Figure S10D).

Given the clear connection between ubiquitination and LCV recruitment observed for Rab1 (Figure 4), we next asked whether Rab5A is present at the LCV at any point during infection. Previous studies conflict on whether Rab5A is recruited to the LCV during WT *L.p.* infection. Initial EM immunogold staining suggested that WT *L.p.* excludes Rab5 from the LCV membrane (Clemens *et al.*, 2000a), but more recent mass spectrometry analysis of purified LCVs and immunofluorescence analysis in RAW macrophages identified Rab5 as LCV localized (Hoffmann *et al.*, 2014). To address this discrepancy in the literature, we carried out immunofluorescence analysis of endogenous Rab5A in HeLa FcγR cells infected with WT or Δ*dotA L.p.* across a time range from 30 min to 5 hpi. We observed clear Rab5A recruitment to both the WT and Δ*dotA* LCV, while the WT LCV still resists lysosomal fusion, as shown by the exclusion of the lysosomal membrane protein Lamp1 (Figure 5, C and D). Interestingly, whereas the Δ*dotA* LCV shows more canonical Rab5A dynamics in which recruitment peaks shortly after internalization and decays quickly thereafter, the WT LCV shows moderate frequencies of Rab5A localization across the first five hours of infection. This mirrors the persistent ubiquitination observed across early infection timepoints (Figure 5A), suggesting that, as for Rab1, Rab5A ubiquitination requires LCV localization. To directly test this hypothesis, we generated mCherry-tagged Rab5A WT and lipid anchor deletion (Rab5A Δ*CAAX*) constructs, and quantified localization to the WT and Δ*dotA* LCVs during infection in HeLa FcγR. Rab5A WT localizes to both the WT and Δ*dotA* LCV, whereas Rab5A Δ*CAAX* is diffuse and excluded from the LCV (Supplemental Figure S10, E and F). Flag-tagged versions of these constructs show a clear loss of monoubiquitination for the Δ*CAAX* construct (Supplemental Figure S10, G and H), consistent with the model that Rab5A monoubiquitination requires membrane association.

We next assessed whether localization of Rab5 to the LCV results in the accumulation of early endosomal markers. Membrane-associated Rab5A recruits early endosome-specific proteins both through direct binding interactions and by the production of the phosphoinositide PI(3)P via the activity of multiple binding partners (Shin *et al.*, 2005). One such protein is early endosome antigen 1 (EEA1), which binds to both active Rab5 and PI(3)P (Simonsen *et al.*, 1998). Despite Rab5 association with the WT LCV, we do not observe recruitment of EEA1 at 1 hpi, while EEA1 robustly localizes to the Δ*dotA* LCV (Figure 5, E and F). Notably, multiple *L.p.* effectors are known to coordinate the conversion of PI(3)P to PI(4)P at the LCV membrane during early infection (Weber *et al.*, 2006; Dong *et al.*, 2016), and the exclusion of EEA1 suggests that this lipid conversion program is active even while Rab5A is present. Conversely, association of Rab5A with the WT LCV is not sufficient to promote an early endosome-like character at the membrane, in contrast to the Δ*dotA* LCV. To determine whether Rab5A activity is detrimental to *L.p.*, we assayed both bacterial replication and lysosomal trafficking of the LCV in the context of Rab5 overexpression. HeLa FcγR transfected with mCherry-Rab5A or mCherry alone were infected with *L.p.* WT or Δ*dotA*, fixed at 4 and 10 hpi, and subjected to immunofluorescence analysis. At 10 hpi, there is a small but significant decrease in the frequency of high bacterial burden LCVs during Rab5A overexpression compared with control (Figure 5G). However, there is no increase in Lamp1-positive WT LCVs at 4 hpi during Rab5A overexpression (Figure 5H), further suggesting that Rab5 recruitment and activity does not promote trafficking of the WT LCV through the endolysosomal pathway.

Bacterial effectors SidC/SdcA are necessary but not sufficient for Rab5A monoubiquitination, and control Rab5A recruitment to the LCV

Next, we sought to identify bacterial effectors required for Rab5A ubiquitination. Previous studies have shown that bacterial effector paralogs SidC and SdcA are required for Rab1 (Horenkamp *et al.*, 2014) and Rab10 (Jeng *et al.*, 2019) ubiquitination. To determine whether SidC/SdcA play similar roles in Rab5 ubiquitination, we infected HEK293T FcγR cells expressing Flag-Rab5A with SidC/SdcA knockout and complemented strains. Indeed, infection with a SidC/SdcA genomic deletion strain (*L.p.* Δ*sidC/sdcA*) fails to induce Rab5A ubiquitination, as indicated by the loss of monoubiquitinated species (Figure 6, A and B). Transformation of the Δ*sidC/sdcA* strain with a plasmid encoding either SdcA or SidC is sufficient to rescue Rab5A monoubiquitination, suggesting that these effectors are functionally redundant in this context. SdcA/SidC have been identified as E3 ligases with unique protein folds (Hsu *et al.*, 2014). While these proteins catalyze autoubiquitination in vitro, neither direct in vitro ubiquitination assays with SidC and Rab1 nor several mass spectrometry–based approaches have revealed host target proteins of SidC/SdcA (Hsu *et al.*, 2014; Shin *et al.*, 2020). In accordance with these findings, ectopic expression of SidC or SdcA in the absence of infection is not sufficient to induce Rab5A monoubiquitination (Figure 6C). This result suggests that the context of infection provides the complete enzymatic machinery required for SidC/SdcA-mediated Rab5 monoubiquitination, which could include either bacterial or host components, or both.

As we have established a link between Rab monoubiquitination and LCV localization, we next examined whether SidC/SdcA control Rab5A recruitment. Immunofluorescence analysis reveals that the Δ*sidC/sdcA* LCV fails to accumulate endogenous Rab5A at 1 hpi, whereas Δ*sidC/sdcA* strains complemented with either SidC- or SdcA-expressing plasmids robustly recruit Rab5A (Figure 6, D and E). The finding that bacterial effectors recruit Rab5A is somewhat surprising, as Rab5 activity is generally thought to be deleterious to *L.p.* infection (Anand *et al.*, 2020; Kim and Isberg, 2023). The Δ*sidC/sdcA* strains are as resistant to lysosomal fusion as WT *L.p.* (Figure 6F), consistent with a model in which Rab5 recruitment and ubiquitination are not a primary mechanism of endosome maturation subversion at the LCV membrane.

SidC/SdcA promote small GTPase ubiquitination beyond the Rab subfamily

With the finding that SidC/SdcA regulate Rab5 ubiquitination, in addition to past work demonstrating their role in Rab1/10 ubiquitination, we hypothesized that SidC/SdcA may promote small GTPase ubiquitination beyond the Rab subfamily. To evaluate the role SidC/SdcA may play in cross-family small GTPase ubiquitination more broadly, we transfected HEK293T FcγR cells with GFP-tagged HRas and RhoA constructs and infected with SidC/SdcA knockout and complemented strains. Strikingly, infection with *L.p.* Δ*sidC/sdcA* abolished ubiquitination of both GTPases, while complementation of *L.p.* Δ*sidC/sdcA* with a plasmid encoding SidC but not SdcA rescued ubiquitination (Figure 6, G and H). Infection with single effector knockout strains Δ*sidC* and Δ*sdcA* recapitulates this phenotype
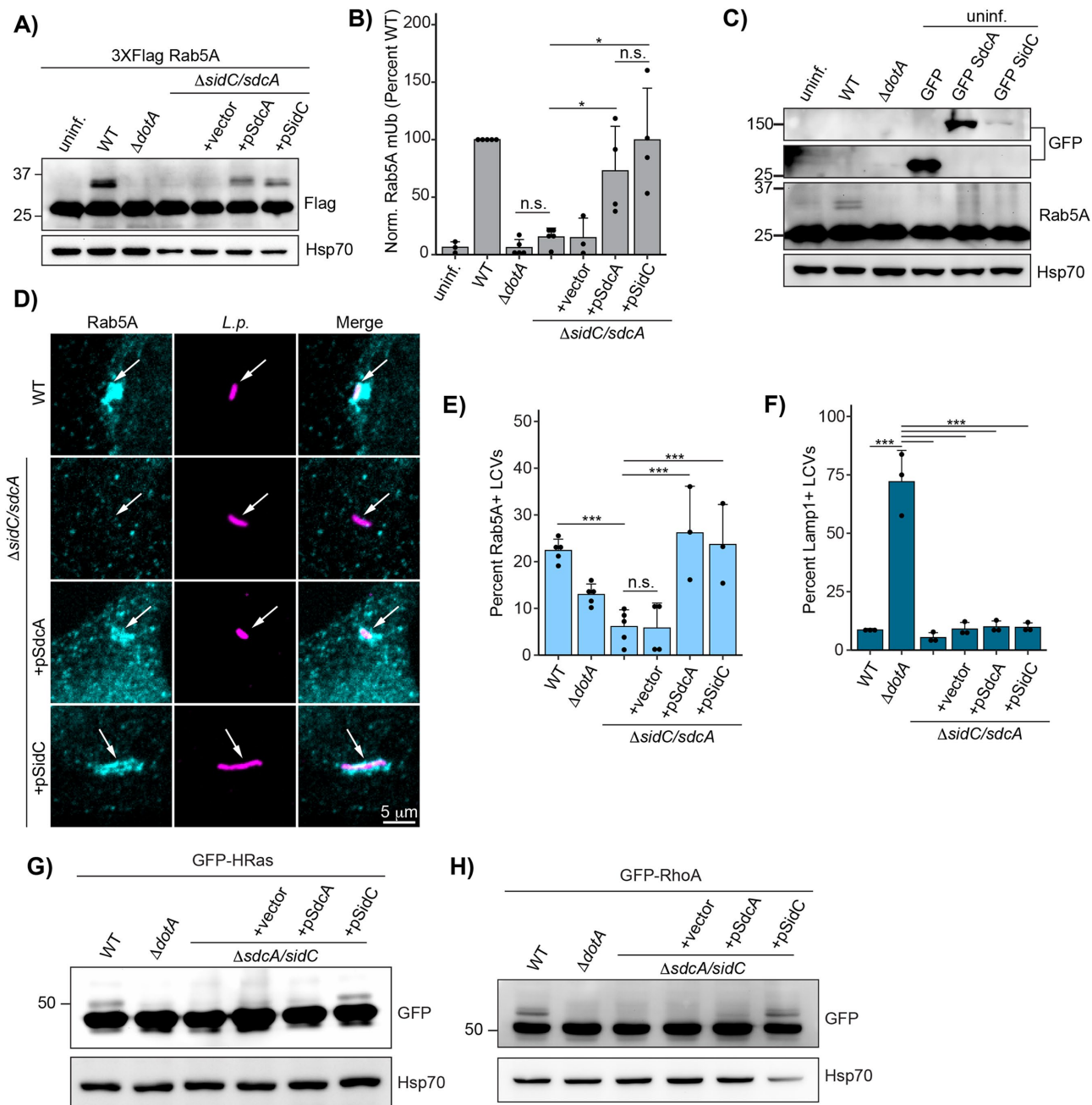
FIGURE 6. Bacterial effectors SidC/SdcA play a central role in small GTPase ubiquitination. (A) Immunoblot analysis of Rab5A monoubiquitination during infection with ΔsidC/sdcA L.p. strain panel (WT, ΔdotA, ΔsidC/sdcA, and ΔsidC/sdcA transformed with vector or plasmid expressing SdcA or SidC). HEK293T FcγR cells transfected with 3XFlag Rab5A were infected with the indicated strain or left uninfected. Cells were lysed at 4 h postinfection and probed with anti-Flag antibody. (B) Quantification of biological replicates (N = 3–5) of experiment shown in (A). Normalized Rab5A monoubiquitination intensity was calculated as a percentage of WT L.p. infection levels (see Materials and Methods), (N = 3–4). (C) Immunoblot analysis of Rab5A monoubiquitination during SdcA or SidC ectopic expression. HEK293T FcγR were either left untransfected (lanes 1–3) or transfected with GFP alone or GFP-tagged SdcA or SidC for 24 h. The untransfected cells were either left uninfected or infected with WT or ΔdotA L.p. (MOI = 20) for 4 h. All cells were lysed and probed with anti-Flag, anti-GFP, and anti-Hsp70 antibodies. (D) Representative images of Rab5A LCV recruitment levels for the ΔsidC/sdcA strain panel as observed by immunofluorescence. HeLa FcγR cells were infected with indicated strain (MOI = 1) for 1 h, fixed, and probed with anti-Legionella and anti-Rab5A antibodies. (E) Quantification of biological replicates (N = 3-5, Bonferroni adjusted p value = 0.003) of experiment shown in (D). 75–150 LCVs were scored per replicate as positive or negative for Rab5A recruitment, and the percent Rab5A+ LCVs was calculated per replicate. (F) Quantification of Lamp1 LCV recruitment for the ΔsidC/sdcA strain panel. HeLa FcγR cells were infected with indicated strain (MOI = 1) for 4 h, fixed, and probed with anti-Legionella and anti-Lamp1 antibodies. LCVs were scored as in (E). (G and H) Ubiquitination of HRas and RhoA is differentially dependent and SidC and SdcA. HEK293T cells transiently expressing the indicated GFP-tagged small GTPase were infected with the ΔsidC/sdcA L.p. strain panel (MOI = 20) as in (A). Cells were infected for 1 h and lysates probed with anti-GFP antibody.

(Supplemental Figure S11, A and B). This result implicates SidC/SdcA in cross-family small GTPase ubiquitination more broadly. It also suggests that SidC/SdcA may play overlapping but distinct roles in small GTPase ubiquitination, as the ubiquitination of Rab1 seems to be primarily dependent upon the activity of SdcA (Horenkamp et al., 2014) (Supplemental Figure S11, C and D), and the ubiquitination of Rab5 appears to be equally dependent upon SidC and SdcA (Figure 6, A and B).

SidE family–mediated polyubiquitination facilitates small GTPase membrane retention

We next sought to identify additional effectors involved in small GTPase ubiquitination. Specifically, we were intrigued by recent work that has linked both the LCV recruitment and ubiquitination of Rab33b to the activity of noncanonical ligase effectors in the SidE family (SidE, SdeA, SdeB, SdeC) (Kawabata et al., 2021), leading us to hypothesize that the SidE family may play similar roles to SidC/SdcA in the recruitment and ubiquitination of small GTPases during infection. To test whether SidE family effectors influence Rab1 and Rab5 ubiquitination, we assessed Rab1/5 ubiquitination in HEK293T FcγR cells infected with WT L.p., ΔdotA, and SidE family knockout or complemented strains. Strikingly, SidE family knockout showed no effect on Rab1 or Rab5 monoubiquitination but diminished high molecular weight polyubiquitinated species (Supplemental Figure S12, A and B). Notably, SidC/SdcA knockout abrogates both mono- and polyubiquitination for Rab5 (Figure 7A) and Rab1 (Supplemental Figure S11C), suggesting that SidE family -mediated polyubiquitination may lie downstream of SidC/SdcA activity.

We next assessed whether the SidE family of effectors is necessary for Rab5 recruitment to the LCV. Immunofluorescence analysis shows that the ΔsidE/sdeABC LCV fails to accumulate endogenous Rab5A at 1 hpi, whereas an ΔsidE/sdeABC strain complemented with SdeB-expressing plasmid robustly recruits Rab5A (Figure 7, C and D). This result suggests that Rab5 monoubiquitination, which is unaffected by the absence of SidE family effectors, is not sufficient to retain Rab5 in the LCV membrane.

With polyubiquitination but not monoubiquitination associated with the retention of Rab5 in the LCV membrane, we hypothesized that polyubiquitinated GTPases may associate more stably with cellular membranes. To test this hypothesis, we performed subcellular fractionations of cells expressing Flag-Rab1 or Rab5 and infected with L.p. WT or ΔdotA. Monoubiquitinated species of both Rabs distributed between the membrane and the cytosol, whereas the higher molecular weight polyubiquitinated species specifically enriched in the membrane fraction (Figure 7, E and F). Taken together, these data are consistent with a model in which SidC/SdcA–mediated monoubiquitination is a prerequisite for Rab5 polyubiquitination by the SidE family of effectors, which in turn anchors the small GTPase to the LCV membrane (Figure 7G).

DISCUSSION

Here, we define the ubiquitinated proteome of HEK293 cells infected with L.p. at 1 and 8 h postinfection. Analysis of this dataset reveals that infection with WT L.p. induces hundreds of significant changes in the host ubiquitinome spanning processes known to be involved in infection, such as membrane trafficking and lipid exchange, as well as processes with less characterized or unknown roles in infection, such as mRNA splicing and solute transport. The most dramatic changes in the host ubiquitinome occur at early timepoints during infection, although substantial modification of the ubiquitinome persists at 8 hpi. Additionally, we see that many of the

same pathways and proteins are targeted throughout infection, suggesting that similar E3 ligases and DUBs may be active throughout infection, or that many early changes in the ubiquitinome are stable. Given the connection between ubiquitination and protein degradation, we also paired our analysis of the host ubiquitinome with an analysis of changes in host protein abundance. Intriguingly, changes in ubiquitination seem to be largely independent of changes in abundance, suggesting that many of the ubiquitination changes we detected during infection are not connected to degradative signaling outcomes.

A major effect of infection was the ubiquitination of 63 of ~163 known small GTPases spanning RAB, RAS, RHO/RAC, RAN, and ARF/SAR subfamilies. We determined that many GTPases are monoubiquitinated during infection, and some are polyubiquitinated. Along with our proteomic data showing no significant small GTPase abundance changes during infection, as well as past work demonstrating that ubiquitinated Rab1 is not degraded in the proteasome (Horenkamp et al., 2014), these results strongly suggest that small GTPase ubiquitination plays a nondegradative role during infection. The cross-family ubiquitination of small GTPases also appears to be specific to L.p. infection, as human cells infected with Salmonella typhimurium or Mycobacterium tuberculosis do not show a comparable level of cross-family ubiquitination (Fiskin et al., 2016; Budzik et al., 2020).

Through sequence alignment and binning of ubiquitinated residues into different structural regions, we were able to determine that most ubiquitination sites fall within GTPase C-terminal regions after the G4 box, including the conserved G5 box SA**K** motif lysine that makes contacts with the guanine of GTP, and the hypervariable C-terminal domain (HVD), which contains sequence elements required for lipidation (Müller and Goody, 2017). Mapping these regions onto the Rab1A structure demonstrated that they form a distinct interface opposite the canonical small GTPase protein-binding regions, Switch I and II. This suggests that GTPase ubiquitination during infection functions through an alternative mechanism of action compared with known PTMs within the Switch regions such as phosphorylation and AMPylation, which are known to block GTPase-protein-binding interactions more directly (Müller et al., 2010; Tan et al., 2011; Aktories and Schmidt, 2014; Levin et al., 2016; Steger et al., 2016).

Although several studies have investigated small GTPase ubiquitination within these non-Switch regions outside the context of infection, the data on downstream consequences are mixed and appear to be highly GTPase and/or residue dependent. Monoubiquitination of RhoC, Rab11a, and KRas on either the G5 SAK motif or the preceding α4 helix appears to be activating (Sasaki et al., 2011; Baker et al., 2013; Lachance et al., 2013; Kholmanskikh et al., 2022), while ubiquitination of Rab5 in the same region appears to impair activity (Shin et al., 2017). Equally paradoxical, ubiquitination of Rab7 in the HVD appears to maintain it in the membrane (Sapmaz et al., 2019), while ubiquitination of H/N/KRas in this region prevents membrane association (Steklov et al., 2018).

We determine that robust recruitment and retention of Rab1 on the LCV promotes its ubiquitination. Infection with either L.p. ΔdrrA or the AMPylation-mutant L.p. ΔdrrA + pDrrA D110,112A, known to have reduced Rab1 recruitment to the LCV, results in a substantial decrease in Rab1 ubiquitination compared with L.p. WT. Conversely, Rab10, which is not recruited to the LCV by DrrA, undergoes ubiquitination at WT levels during infection with DrrA-deficient strains. This result indicates that Rab1 recruitment is required for its ubiquitination, and that ubiquitination of other small GTPases is not contingent upon DrrA activity or Rab1 LCV association.
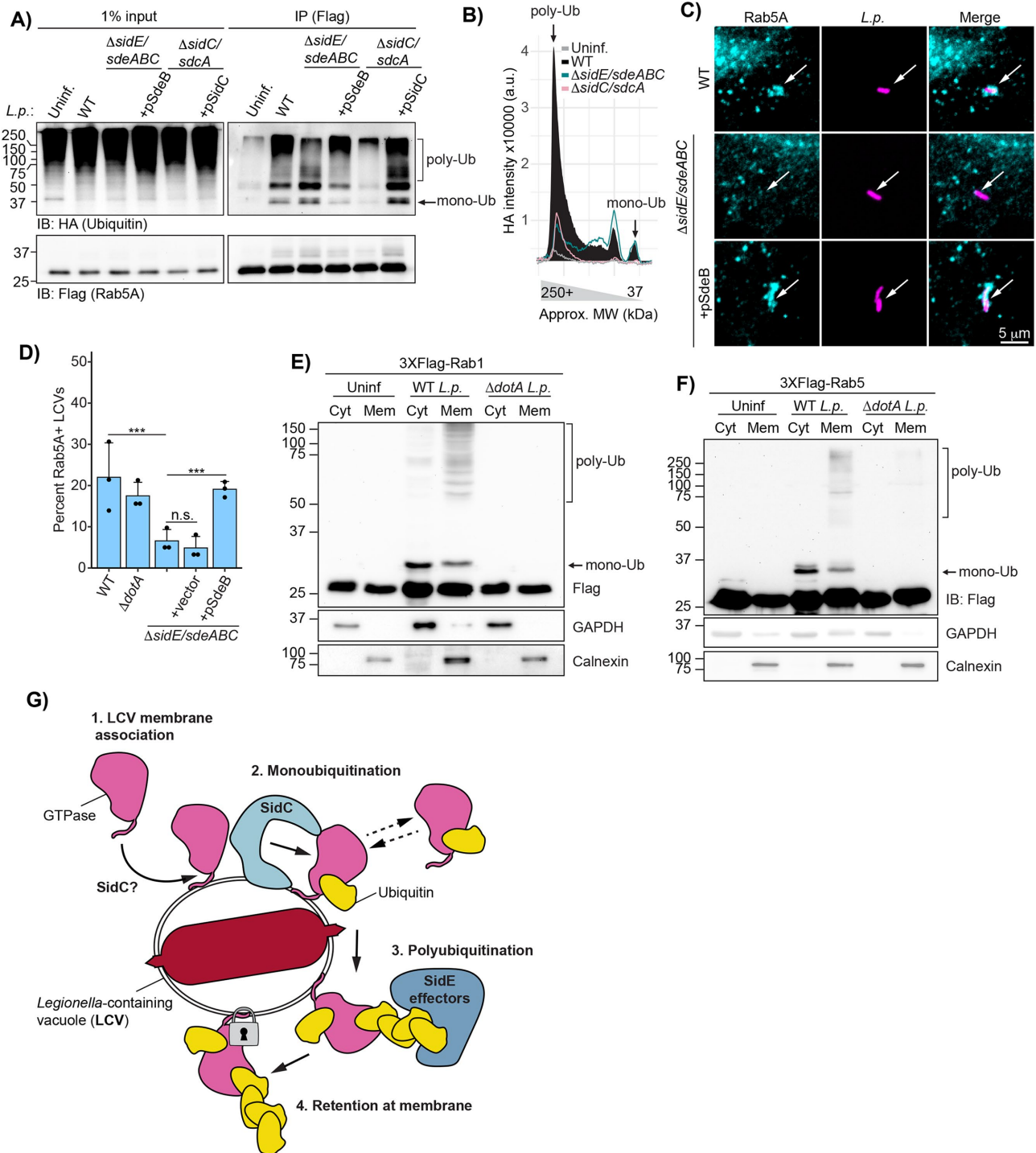
FIGURE 7. SidE family mediated polyubiquitination is downstream of monoubiquitination and anchors Rabs to the membrane. (A) Immunoblot analysis of Flag-Rab5A immunoprecipitation from cells infected with SidE family and SidC/SdcA strain panel. HEK293T FcγR cells transfected with 3XFlag Rab5A and HA-ubiquitin were infected with *L.p.* WT, Δ*sidE/sdeABC*, Δ*sidC/sdcA*, and appropriate plasmid complemented strains (MOI = 20) for 4 h or left uninfected. After Flag pulldown, input and IP samples were probed with anti-HA and anti-Flag antibodies. (B) Plot profiles of HA signal shown in IP panel in (A) for uninfected and *L.p.* WT, Δ*sidE/sdeABC*, and Δ*sidC/sdcA* infected samples. (C) Representative images of Rab5A LCV recruitment levels for the Δ*sidE/sdeABC* strain panel as observed by immunofluorescence. HeLa FcγR cells were infected with indicated strain for 1 h, fixed, and probed with anti-*Legionella* and anti-Rab5A antibodies. (E) Quantification of biological replicates (*N* = 3, Bonferroni adjusted *p* value = 0.005) of experiment shown in (D). 60–120 LCVs were scored per replicate as positive or negative for Rab5A recruitment, and the percent Rab5A+ LCVs was calculated per replicate. (E and F) Immunoblot analysis of cellular fractionations performed on HEK293T FcγR cells transiently expressing the indicated Flag-tagged Rab and infected with *L.p.* WT or Δ*dotA* (MOI = 20) or left uninfected. Cells were infected for 1 (E) or 4 (F) hours. (G) Schematic of working model of small GTPase mono- and polyubiquitination.

Paired with our Rab1 LCV-recruitment model, the observation that all Rab5 isoforms are ubiquitinated during infection led us to the finding that Rab5A is recruited to the WT LCV during infection. Previously published results conflict on whether Rab5 associates with the WT LCV (Clemens *et al.*, 2000a; Hoffmann *et al.*, 2014). In the present study, we relied on immunofluorescence analysis of endogenous Rab5 during infection and found that the WT LCV stains positive for Rab5A at moderate frequencies throughout early infection. Additionally, we link Rab5 ubiquitination to LCV recruitment, and observe ubiquitination of endogenous Rab5 in U937 macrophage-like cells. Notably, previous reports suggest that overexpression of Rab5 antagonizes *L.p.* pathogenesis but does so by decreasing the integrity of the LCV membrane (Anand *et al.*, 2020; Kim and Isberg, 2023), rather than by increasing trafficking of the LCV to the lysosome. Consistent with this finding, we observe that Rab5A overexpression results in a bacterial replication defect without an increase in Lamp1 recruitment to the WT LCV. Taken together, these results are inconsistent with a model by which Rab5 activity simply increases trafficking of the LCV to the lysosome, and instead suggest a nuanced interplay between *L.p.* effectors and Rab5 activity during infection.

Our data place the ubiquitin ligase bacterial effectors SidC and SdcA at the center of cross-family small GTPase ubiquitination, although the specific role that they play is still unclear. We find that SidC/SdcA are required for both Rab5A LCV recruitment and ubiquitination. This result adds Rab5A to the list of GTPases already known to be LCV recruited by SidC/SdcA (Arf1, Rab10), and GTPases whose ubiquitination is known to be controlled by SidC/SdcA (Rab1, Rab10) (Horenkamp *et al.*, 2014; Jeng *et al.*, 2019). Here, we show that the ubiquitination of HRas and RhoA is also dependent upon the activity of SidC/SdcA.

Despite their involvement in the recruitment and ubiquitination of these diverse small GTPases, several lines of evidence suggest that small GTPases may not be a direct target of SidC/SdcA ubiquitin ligase activity. First, ectopic expression of SidC/SdcA does not induce ubiquitination of Rab1 (Horenkamp *et al.*, 2014; Hsu *et al.*, 2014) or Rab5 (this study). Second, in vitro ubiquitination reactions containing purified SidC have not resulted in Rab1A ubiquitination (Hsu *et al.*, 2014). Lastly, protein–protein interaction experiments have failed to detect interaction between SidC/SdcA and Rab1, Arf1, or numerous other proteins involved in LCV formation (Horenkamp *et al.*, 2014). We cannot rule out the possibility that SidC/SdcA may be activated by or act in complex with another bacterial or host cell protein during infection in order to directly catalyze cross-family small GTPase ubiquitination.

Intriguingly, we note that SidC and SdcA contribute differentially towards the ubiquitination of various GTPases. We find that SdcA is primarily responsible for Rab1 ubiquitination, SidC is primarily responsible for HRas, and RhoA ubiquitination, and both SidC and SdcA seem to play equivalent roles in promoting Rab5 ubiquitination. This difference in specificity implies that SidC and SdcA may target different membranes or GTPases for recruitment to the LCV, consistent with past work that has found lower conservation in a domain of SidC/SdcA hypothesized to be involved in membrane tethering (Horenkamp *et al.*, 2014).

We find that the SidE family of bacterial effectors contribute to high molecular weight polyubiquitination – but not monoubiquitination – of the GTPases Rab1/5, and that polyubiquitinated Rab1/5 is membrane associated. Combined with the observation that the SidE family is required for Rab5 recruitment to the LCV, these data leads us to hypothesize that cross-family small GTPase ubiquitination is at least in part a means to retain GTPases in the bacterial vacuole membrane. Recent work on a *L.p.* effector DUB, Lem27/LotC, is consistent with this model, showing that overexpression of Lem27/LotC reduces both poly- and monoubiquitination of Rab10 during infection, and also suppresses Rab10 association with the LCV (Liu *et al.*, 2020). SidE-mediated polyubiquitination appears to occur downstream of initial recruitment and monoubiquitination, as manipulations such as knockout of the Rab1 GEF effector DrrA, deletion of CAAX box residues, and knockout of SidC/SdcA all affect the accumulation of mono- and polyubiquitinated species together. Notably, knockout of SidE/SdeA/B/C does not completely prevent polyubiquitination of Rab5 (Figure 7A), indicating that other effectors play a role in polyubiquitination. However, the Δ*sidE/sdeABC* strain LCV is largely Rab5-negative, suggesting that noncanonical PR-ubiquitination may play a specific role in maintaining Rab5 at the LCV membrane.

We note that there are differences in the recruitment and ubiquitination cascades that regulate Rab1 and Rab5: While SidC/SdcA and SidE/SdeA/B/C regulate the mono- and polyubiquitination of Rab1, the role that they play in its LCV localization is unclear, as numerous effectors, including DrrA, regulate Rab1 recruitment and retention in the LCV membrane (Ingmundson *et al.*, 2007; Mukherjee *et al.*, 2011; Neunuebel *et al.*, 2012; Hardiman and Roy, 2014). Indeed, past work demonstrates that SidC/SdcA do not recruit Rab1 to the LCV membrane (Horenkamp *et al.*, 2014). For Rab5, however, the SidC/SdcA-SidE family ubiquitination cascade appears to be primarily responsible for Rab5 recruitment and retention.

Our data lead us to propose a model in which: 1) initial recruitment of small GTPases to the LCV membrane, which may be mediated by SidC/SdcA, precedes 2) monoubiquitination, for which SidC/SdcA are required, priming these LCV-localized small GTPases for 3) SidE-mediated polyubiquitination, that leads to 4) their retention in the membrane (Figure 7G). This work suggests a complex interplay between SidC/SdcA and the SidE effector family in the ubiquitination and LCV retention of small GTPases during infection, and more broadly implies a collaboration between these two effector groups in modulating ubiquitin signaling. Our findings position *L.p.* as a tool to understand a small GTPase regulation in both infected and uninfected contexts. Further examination of the host and bacterial proteins required for cross-family small GTPase ubiquitination is warranted, as the mechanistic details of this phenomenon will provide insight into both eukaryotic regulation of small GTPase activity and bacterial strategies of host cell manipulation.

MATERIALS AND METHODS
Request a protocol through *Bio-protocol.*

Cell lines
HEK293T cells (female), HEK293 cells (female) stably expressing the Fcγ receptor IIb (HEK293 FcγR cells), and HeLa FcγR cells were cultured in Dulbecco's Modified Eagle's Medium (DMEM, GIBCO) containing 10% FBS (VWR) at 37°C and 5% CO$_2$. FcγR-expressing cell lines were gifts from the lab of Dr. Craig Roy at Yale University. U937 cells (a gift from Dr. Michael Bassik at Stanford University) were cultured in RPMI-1640 (Corning) supplemented with 10% heat-inactivated FBS (VWR). U937 were differentiated into macrophage-like cells in 20 ng/ml phorbol 12-myristate 13-acetate (Sigma) for 72 h, then replated in media without PMA and allowed to rest for 48 h before *L.p* infection.

Bacterial strains and plasmids
Experiments were performed with *L.p.* serogroup 1, strain Lp01 or Lp02. Avirulent T4SS-null strains were derived as previously

described (Berger and Isberg, 1993; Berger *et al.*, 1994). *L.p.* strains were grown on Charcoal Yeast Extract (CYE) agar plates or AYE broth supplemented with (FeNO$_3$ 0.135 g/10 ml) and cysteine (0.4 g/10 ml). Growth media for Lp02 thymidine auxotroph-derived strains was supplemented with 100 µg/ml thymidine. For strains carrying complementation plasmids, chloramphenicol (5 µg/ml) was supplemented for plasmid maintenance, and IPTG (1 mM) was added for 2 h of induction prior to infection. The unmarked gene deletion Δ*sidC-sdcA* and Δ*drrA* strains were derived from the parental strain using allelic exchange as described previously (Berger *et al.*, 1994). Rab5A, Rab5B, and Rab5C coding sequences were amplified from HeLa cDNA and cloned into a pcDNA3.1 mammalian expression vector containing the appropriate N-terminal tag (3XFlag or mCherry). Rab5A, Rab1A, and Rab10 CAAX deletion inserts were derived from appropriate full-length plasmid by PCR amplification of the desired region.

Infection of cultured mammalian cells with *L.p.*

Infections with *L.p.* were performed as previously described (Treacy-Abarca and Mukherjee, 2015). *L.p.* heavy patches grown for 48 h on CYE plates were either used directly for infection, or for overnight liquid cultures in AYE medium until reaching an OD$_{600}$ of 3. *L.p.* from the overnight culture was enumerated and the appropriate amount was opsonized with *L.p.*-specific antibodies at a dilution of 1:2000 in cell growth medium for 20 min. HEK293 FcγR were grown on poly-lysine–coated cell culture plates to a confluency of 80% and infected with the *L.p.* WT strain or the isogenic Δ*dotA*-mutant strain at a multiplicity of infection (MOI) of 1–100 as indicated. The infection was synchronized by centrifugation of the plates at 1000 × *g* for 5 min. To prevent internalization of any remaining extracellular bacteria at later timepoints, cells were washed three times with warm PBS after 1 h of infection and fresh growth medium was added. Cells were collected for down-stream processing at the indicated timepoints. Uninfected samples used as controls for infection experiments were mock-infected using media and opsonization antibody only.

Sample preparation for proteomics analysis

HEK293 FcγR infected for 1 or 8 h with the *L.p.* WT strain Lp01 or the isogenic Δ*dotA* mutant were infected at an MOI of 100. Uninfected HEK293 FcγR cells were included as a control. Cells were washed with ice-cold PBS, collected, and the pellet was frozen at –80°C. Cell pellets were lysed by probe sonication in three pulses of 20% amplitude for 15 s in a lysis buffer consisting of: 8 M urea, 150 mM NaCl, 100 mM ammonium bicarbonate, pH 8; added per 10 ml of buffer: 1 tablet of Roche mini-complete protease inhibitor EDTA free and 1 tablet of Roche PhosSTOP. To remove insoluble precipitate, lysates were centrifuged at 16,100 × *g* at 4°C for 30 min. A Bradford Assay (Thermo Fisher Scientific) was performed to measure protein concentration in cell lysate supernatants. Six milligrams of each clarified lysate was reduced with 4 mM tris(2-carboxyethyl)phosphine for 30 min at room temperature and alkylated with 10 mM iodoacetamide for 30 min at room temperature in the dark. The remaining alkylated agent was quenched with 10 mM 1,4-dithiothreitol for 30 min at room temperature in the dark. The samples were diluted with three starting volumes of 100 mM ammonium bicarbonate, pH 8.0, to reduce the urea concentration to 2 M. Samples were incubated with 50 µg of sequencing grade modified trypsin (Promega) and incubated at room temperature with rotation for 18 h. The sample pH was reduced to ~2.0 by the addition of 10% trifluoroacetic acid (TFA) to a final concentration of 0.3% trifluoroacetic acid. Insoluble material was removed by centrifugation at 16,000 × *g* for

10 min. Peptides were desalted using SepPak C18 solid-phase extraction cartridges (Waters). The columns were activated with 1 ml of 80% acetonitrile (I), 0.1% TFA, and equilibrated three times with 1 ml of 0.1% TFA. Peptide samples were applied to the columns, and the columns were washed three times with 1 ml of 0.1% TFA. Peptides were eluted with 1.2 ml of 50% I, 0.25% formic acid. Peptides were divided for global protein analysis (10 µg) or diGly-enrichment (remaining sample), and lyophilized.

diGly peptide enrichment by immunoprecipitation

Peptide samples were subjected to ubiquitin remnant immunoaffinity. Ten microliters of PTMScan® Ubiquitin Remnant Motif (K-ε-GG) Antibody Bead Conjugate purification (Cell Signaling Technology) slurry was used per 1 mg peptide sample. Ubiquitin remnant beads were washed twice with IAP buffer, then split into individual 1.7 ml low bind tubes (Eppendorf) for binding with peptides. Peptides were dried with a centrifugal evaporator for 12 h to remove TFA in the elution. The lyophilized peptides were resuspended in 1 ml of IAP buffer (50 mM 4- morpholinepropnesulfonic acid, 10 mM disodium hydrogen phosphate, 50 mM sodium chloride, pH 7.5). Peptides were sonicated and centrifuged for 5 min at 16,100 × *g*. The soluble peptide supernatant was incubated with the beads at 4°C for 90 min with rotation. Unbound peptides were separated from the beads after centrifugation at 700 × *g* for 60 s. Beads containing peptides with diGly remnants were washed twice with 500 µl of IAP buffer, then washed twice with 500 µl of water, with a 700 × *g* 60-s centrifugation to allow the collection of each wash step. Peptides were eluted twice with 60 µl of 0.15% TFA. diGly remnant peptides were desalted with UltraMicroSpin C18 column (The Nest Group). Desalted peptides were dried with a centrifugal adaptor and stored at –20°C until analysis by liquid chromatography and mass spectrometry.

Mass spectrometry data acquisition and processing

Samples were resuspended in 4% formic acid, 4% acetonitrile solution, separated by a reverse-phase gradient over a nanoflow column (360 µm O.D. × 75 µm I.D.) packed with 25 cm of 1.8 µm Reprosil C18 particles with (Dr. Maisch), and directly injected into an Orbitrap Fusion Lumos Tribrid Mass Spectrometer (Thermo Fisher Scientific). Total acquisition times were 120 min for protein abundance, 100 min for phosphorylation, and 70 min for ubiquitylation analyses. Specific data acquisition settings are detailed in Supplemental Table S1. Raw MS data were searched with MaxQuant against both the human proteome (UniProt canonical protein sequences downloaded January 11, 2016) and the *Legionella Pneumophila Philadelphia* proteome (downloaded July 17, 2017). Peptides, proteins, and PTMs were filtered to 1% false discovery rate in MaxQuant (Cox *et al.*, 2014). PCA of normalized MS intensities of experimental conditions (control, Δ*dotA*-1 h, Δ*dotA*-8 h, WT-1 h, WT-8 h) was performed using the factoextra R package as implemented by the artMS bioconductor package. The plot illustrates the relationship between the variables (conditions) and the principal components, where each variable is represented as a vector, and the direction and length of the vectors indicate how each variable contributes to the two principal components. Two vectors close together indicates a strong positive correlation between those two variables, that is, they contribute to the principal components in a similar way. Statistical analysis of quantifications obtained from MaxQuant was performed with the artMS Bioconductor package (version 0.9) (Jimenez-Morales *et al.*, 2019). Each dataset (proteome and ubiquitinome) was analyzed independently. Quality control plots were generated using the artMS quality control functions. The site-specific relative quantification of posttranslational modifications required a preliminary

step consisting of providing the ptm-site/peptide-specific annotation ("artmsProtein2SiteConversion()" function). artMS performs the relative quantification using the MSstats Bioconductor package (version 3.14.1) (Choi *et al.*, 2014). Contaminants and decoy hits were removed. Samples were normalized across fractions by median-centering the Log$_2$-transformed MS1 intensity distributions (Figure 1; Supplemental Figures S1B and S3B).

Imputation strategy

Log2FC for protein/sites with missing values in one condition but found in ≥2 biological replicates of the other condition of any given comparison were estimated by imputing intensity values from the lowest observed MS1 intensity across sample peptides (Webb-Robertson *et al.*, 2015); *p* values were randomly assigned between 0.05 and 0.01 for illustration purposes.

Subcellular compartment analysis, functional enrichment analysis, and small GTPase sequence alignment

Statistically significant changes were selected by applying the joint thresholds of $|Log2FC| \geq 1$, adjusted-*p* value < 0.05. Imputed values were also considered significant and are indicated in figures separately from nonimputed values. WT1 h-Control, WT8 h-Control, $\Delta dotA$1 h-Control, and $\Delta dotA$8 h-Control comparisons were filtered using these significance criteria for subsequent analyses. Subcellular compartment analysis was performed by tabulating the number of significantly regulated proteins per compartment based on subcellular localization identifiers from UniProt. Biological pathway and protein complex enrichment was performed using Metascape (Zhou *et al.*, 2019) (https://metascape.org). The following ontology sources were used for analysis: GO Biological Processes, KEGG Pathway, GO Molecular Functions, GO Cellular Components, Reactome Gene Sets, Hallmark Gene Sets, Canonical Pathways, BioCarta Gene Sets, CORUM, WikiPathways and PANTHER Pathway. Significant enrichment terms were selected using the combined thresholds of *p* value < 0.01, a minimum count of 3 proteins, and an enrichment factor > 1.5. Proportional Venn diagrams were created using DeepVenn (Hulsen, 2022) and recolored in Adobe Illustrator. Proteins within the Ras superfamily were defined based on the "Ras small GTPase superfamily" definition in the HUGO Gene Nomenclature Committee database (https://www.genenames.org/, HGNC group ID = 358). Sequence alignment was performed using Jalview (Waterhouse *et al.*, 2009).

Cell lysis, immunoprecipitation, and immunoblot analysis

HEK293 FcγR cells grown on poly-lysine–coated plates were treated as indicated, washed three times with ice-cold PBS and harvested with a cell scraper. Cells were pelleted at $3000 \times g$ for 10 min at 4°C. For preparation of whole-cell lysates, cell pellets were resuspended in RIPA buffer supplemented with cOmplete Protease Inhibitor Cocktail (Roche), PMSF (1 mM), and 10 mM NEM and lysed under constant agitation for 20 min at 4°C. Cell debris was removed by centrifugation at $16,000 \times g$ for 20 min at 4°C. Protein concentration was measured using the Pierce 660 nm Protein Assay Kit or the Pierce™ BCA Protein Assay Kit (Thermo Fisher Scientific). For each sample, 20–30 µg of proteins were denatured in SDS sample buffer/5% β-mercaptoethanol at 95°C for 5 min. For Flag pull-down assays, cells were lysed in 137 mM NaCl, 20 mM Tris base pH 8, 1% vol/vol NP40, 2 mM EDTA supplemented with inhibitors as above. Protein concentrations were measured as above, and lysates were diluted to equal volumes at equal concentrations (1–3 mg/ml). Input samples were removed and prepared for SDS–PAGE as above. Anti-Flag M2 antibody was added at a 1:50 dilution to the remaining

lysate and rotated overnight at 4°C. Samples were incubated with rotation with Invitrogen Dynabeads Protein G (1.5 mg/sample) for 2 h at 4°C. Beads were washed three times with ice-cold lysis buffer, and bound proteins were eluted in 30 µl 2X SDS sample buffer for 10 min at 95°C. For ubiquitin pull-down assays using the SignalSeeker kit (Cytoskeleton Inc), cells were lysed in provided BlastR buffer with protease inhibitor and NEM, and total protein concentration measured using Precision Red Advanced protein assay. Lysates were diluted to 1 mg/ml, and 1 ml of diluted lysate was incubated with either unconjugated (control) or ubiquitin binding domain–conjugated beads for 2 h at 4°C on a rotating platform. Beads were washed three times in wash buffer, and bound proteins were eluted using kit spin columns. For immunoblot analysis, samples were loaded on 8–12% SDS-polyacrylamide gels and separated by SDS–PAGE. Proteins were transferred to polyvinylidene difluoride membranes (0.45 µm, Millipore) at 30 V, 4°C for 16 h. For total ubiquitin blots (Figure 1D), total protein was quantified before blocking using Invitrogen No-Stain Protein Labeling Reagent. Membranes were washed with PBS-T (PBS/ 0.1% Tween-20 [Thermo Fisher Scientific]), blocked with 5% Blotting Grade Blocker Non Fat Dry Milk (Bio-Rad) for 1 h at room temperature, and incubated with the primary antibodies diluted in blocking buffer/0.02% (wt/vol) sodium azide overnight at 4°C. Membranes were washed three times with PBS-T and incubated with Goat Anti-Mouse IgG (H+L) HRP Conjugate (Thermo Fisher Scientific), Goat Anti-Rabbit IgG (H+L) (Thermo Fisher Scientific), HRP Conjugate, diluted at 1:5000 in blocking buffer for 60 min at room temperature. After three washes with PBS-T, membranes were incubated with Amersham ECL Western Blotting Detection Reagent (Global Life Science Solutions) for 1 min and imaged on a ChemiDoc Imaging System (Bio-Rad).

Cellular fractionation

After indicated treatment, cells were collected by gentle scraping into the culture medium and pelleted at $200 \times g$ for 5 min at 4°C. Cells were washed in ice-cold 1X PBS, then gently homogenized in ice-cold homogenization buffer (150 mM KCl, 20 mM HEPES pH 7.4, 2 mM EDTA, 1X cOmplete Protease Inhibitor Cocktail). Cells were lysed with 20–30 passes through a 25-g needle. Lysates were spun at $0.6 \times g$, 4°C for 5 min to remove nuclei and unlysed cells. Postnuclear supernatant was spun at $150,000 \times g$ for 45 min, and the supernatant transferred to a new tube (cytosolic fraction). The membrane pellet was washed once in homogenization buffer and repelleted at $150,000 \times g$, 4°C for 20 min. The supernatant was removed, and the membrane pellet resuspended in homogenization buffer + 1% vol/vol Triton-X 100.

Immunoblot quantification

Images were exported from ImageLab (Bio-Rad) as 16-bit tiff and analyzed in ImageJ. Plot profiles were generated for each lane and the integrated density was calculated using the ImageJ built in gel analyzer tools. Total ubiquitin signal was normalized to total protein, and the fold change was calculated compared with the appropriate uninfected control. To calculate normalized Rab monoubiquitination intensity, integrated density was measured for the unmodified band at subsaturated exposure. Integrated density was measured for the higher molecular weight monoubiquitination band at the lowest exposure in which this band was visible. Normalized Rab monoubiquitination was calculated as follows: IntDen monoUb/(IntDen monoUb + InDen unmod Ub). To standardize these values across biological replicates, values are represented as a percentage of the WT infection condition for each replicate. The intensity profiles in Figure 7B were generated in Fiji.

Immunofluorescence, image acquisition, and image analysis

HeLa FcγR cells were grown on poly-lysine–coated coverslips in 24-well cell culture plates. Cells were treated as indicated, washed three times with PBS, and fixed in 4% paraformaldehyde/PBS for 15 min at room temperature. Cells were then treated with 2% BSA, 0.5% saponin in PBS (blocking/permeabilization buffer) for 1 h at room temperature (RT). Cells were stained with primary antibodies diluted in blocking/permeabilization buffer overnight at 4°C, washed three times with PBS, and stained with secondary antibodies diluted in blocking/permeabilization buffer for 1 h at RT. Cells were then stained with Hoechst33342 at 1:2000 in PBS for 10 min and washed three times with PBS. Coverslips were dipped three times into purified ddH$_2$O to remove salts, dried, and mounted on microscopy glass slides with Prolong Diamond antifade 5 (Thermo Fisher Scientific). Slides were cured overnight at room temperature. Images were acquired on a Nikon Ti2 Eclipse inverted microscope outfitted with a CREST X-Light V2 spinning disk unit and Photometrics Prime 95B CMOS camera (binning 1 × 1, 16-bit). All images were acquired using a 60 × 1.4NA oil immersion objective. NIS-Elements software was used to control the microscope and acquire images. Lasers were used at the following intensities: ExW 365 nm 25%, ExW 488 nm 25%, ExW 561 nm 100%, ExW 640 nm 100%. Exposure time ranged from 10 to 50 ms. Images were analyzed in Fiji. Experimental conditions were blinded either before image acquisition, or before image analysis using the Fiji Blind Analysis Tools plugin filename encrypter. For LCV scoring, max intensity Z projections were generated. LCVs were scored positive if the LCV region was visible in the protein marker of interest channel only (i.e., without the *L.p.* marker). All LCV area measurements were carried out in Fiji using the freehand selection tool. Representative images in all figures are max intensity Z projections.

Cell transfections

All transfections were performed with jetPRIME (Polyplus). HEK293 FcγR or HeLa FcγR cells were grown to 60% confluency and transfected according to the manufacturer's recommendations. For transfection of plasmid DNA, 0.25 µg DNA was used for 24-well plates, 1–2 µg DNA for 6-well plates, 2–3 µg for 60-mm plates, and 5–10 µg for 100-mm plates. Twenty-four hours after transfection, cells were treated as indicated and analyzed or harvested. For experiments in which HA-ubiquitin was transiently coexpressed, the expression construct was added at 20% of the total amount of DNA to minimize pleiotropic effects of strong ubiquitin overexpression.

Statistical analysis and data representation

Plots were generated in Prism or in R using the ggplot2 package. All bar graphs represent the mean value across biological replicates, and individual values for each replicate are shown for N<10. Individual points in line graphs in Figure 5 represent mean values across biological replicates. Error bars on bar and line graphs represent SD. For all Western blot quantification, data were subjected to a one-way ANOVA followed by a Tukey–Kramer post-hoc test for each pair of means (* = $p < 0.05$, n.s. = $p \geq 0.05$). For LCV scoring, G test of independence was performed on pooled counts for each nominal measurement variable (positive vs. negative, or replication bin vs. total) and experimental condition from all biological replicates. Upon verifying significance ($p < 0.05$), data from experiments with more than two conditions (e.g., multiple strains) was subjected to pairwise comparisons between conditions by post-hoc G-test using a Bonferroni-adjusted p value as a significance threshold as indicated in figure legend. For all G tests, n.s. = $p \geq$ threshold, * = $p <$ threshold, ** = $p <$ threshold $\times 10^{-1}$, *** = $p <$ threshold $\times 10^{-2}$.

Key Resources

Key resources used in generation of this research are listed in Table 1.

Cell lines		
Cell Line	**ID**	**Source**
Human: HEK293 cells stably expressing FcγRIIb	derived from ATCC CRL-1573	Gift from Dr. Craig Roy
Human: HEK293T cells stably expressing FcγRIIb	derived from ATCC CRL-3216	This study
Human: HeLa cells stably expressing FcγRIIb	derived from ATCC CCL-2	Gift from Dr. Craig Roy
Human: U937	ATCC CRL-1593.2	Gift from Dr. Michael Bassik
Bacterial Strains		
Strain	**ID**	**Source**
Legionella pneumophila serogroup 1 strain Lp01	LEG001	(Berger *et al.*, 1994), Gift from Dr. Craig Roy
Lp01 Δ*dotA*	LEG002	(Berger *et al.*, 1994), Gift from Dr. Craig Roy
Lp01 Δ*drrA*	LEG005	Gift from Dr. Craig Roy
Lp01 Δ*drrA* pJB1806	LEG169	This study
Lp01 Δ*drrA* pJB1806::DrrA	LEG045	This study
Lp01 Δ*drrA* pJB1806::DrrA D110, 112A	LEG046	This study
Lp01 Δ*sidC/sdcA* (Δ*lpg2510-2511*)	LEG073	Gift from Dr. Craig Roy
Lp01 Δ*sidC/sdcA* pJB1806	LEG184	This study
Lp01 Δ*sidC/sdcA* pJB1806::SdcA	LEG081	This study
Lp01 Δ*sidC/sdcA* pJB1806::SidC	LEG082	This study

TABLE 1: Key resources.

Bacterial Strains		
Strain	**ID**	**Source**
Legionella pneumophila serogroup 1 strain Lp02 *rpsL hsdR thyA*	LEG003	(Berger and Isberg, 1993), Gift from Dr. Craig Roy
Lp02 Δ*dotA* (LP03)	LEG004	(Berger and Isberg, 1993), Gift from Dr. Craig Roy
Lp02 Δ*sidC/sdcA* (Δ*lpg2510-2511*)	LEG173	This study
Lp02 Δ*sidC/sdcA* pJB1806	LEG179	This study
Lp02 Δ*sidC/sdcA* pJB1806::SdcA	LEG180	This study
Lp02 Δ*sidC/sdcA* pJB1806::SidC	LEG181	This study
Lp02 Δ*sidE* Δ*sdeC* Δ*sdeBA* (Δ*lpg0234*, Δ*lpg2153* Δ*lpg2156-2157*), annotated as "Δ*sidE/sdeABC*" for brevity	LEG151	(Jeong *et al.*, 2015), Gift from Dr. Ralph Isberg
Lp02 Δ*sidE* Δ*sdeC* Δ*sdeBA* pJB1806	LEG170	This study
Lp02 Δ*sidE* Δ*sdeC* Δ*sdeBA* pJB1806::SdeB	LEG171	This study
Recombinant DNA		
Vector	**ID**	**Source**
pEGFP-N1 Arf1-GFP	pSM114	Gift from Dr. Craig Roy
pEGFP-N1 Arf6-GFP	pSM115	Gift from Dr. Craig Roy
pCDNA3.1 3XFlag-Rab1 WT	pSM178	This study
pCDNA3.1 3XFlag-Rab1 ΔCAAX	pSM183	This study
pcDNA3.1 EGFP-Rab1 WT	pSM234	This study
pcDNA3.1 EGFP-Rab1 ΔCAAX	pSM236	This study
pCDNA3.1 3XFlag-Rab10 WT	pSM184	This study
pCDNA3.1 3XFlag-Rab10 ΔCAAX	pSM186	This study
pEGFP-C1 GFP-Rab6A	RC45	Gift from Dr. Craig Roy
pEGFP-C1 GFP-Rab9A	RC57	Gift from Dr. Craig Roy
pEGFP-C1 GFP-Rab19	RC66	Gift from Dr. Craig Roy
pEGFP-C1 GFP-Rab20	RC69	Gift from Dr. Craig Roy
pEGFP-C1 GFP-Rab35	RC77	Gift from Dr. Craig Roy
pXFP mCerulean3-Rap1	pSM259	Addgene #134928
pEGFP-C1 GFP-Rap2B	pSM258	Addgene #118321
pCI mEGFP-HRas	pSM253	Addgene #18662
pEGFP-C3 GFP-RhoA	pSM254	Addgene #23224
pEGFP-C2 GFP-RhoB	pSM255	Addgene #23225
pEGFP-C2 GFP-RhoC	pSM256	Addgene #23226
pEGFP-C GFP-RhoQ	pSM257	Addgene #23232
pcDNA3.1 mCherry-Rab5A	pAS042	This study
pcDNA3.1 mCherry-Rab5A ΔCAAX	pAS049	This study
pcDNA3.1 3XFlag-Rab5A	pAS034	This study
pcDNA3.1 3XFlag-Rab5A ΔCAAX	pAS041	This study
pcDNA3.1 3XFlag-Rab5B	pAS050	This study
pcDNA3.1 3XFlag-Rab5C	pAS051	This study
pEGFP-C2	pSM150	Gift from Dr. Craig Roy
pEGFP-C2 GFP-SdcA	pSM261	Gift from Dr. Craig Roy
pEGFP-C2 GFP-SidC	pSM174	Gift from Dr. Craig Roy
pRK5-HA Ubiquitin	pSM099	Gift from Dr. Kohei Arasaki

TABLE 1: Key resources. Continues

Antibodies		
Antigen	**Dilution (application)**	**Source**
Rab5A	1:1000 (WB), 1:200 (IF)	Cell Signaling Technology (46449)
EEA1	1:100 (IF)	Abcam (ab70521)
Lamp1	1:200 (IF)	Cell Signaling Technology (15665)
Flag	1:2500 (WB), 1:50 (IP)	Sigma (F1804)
Flag (HRP conjugate)	1:2500 (WB)	Sigma (A8592)
Hsp70	1:2000 (WB)	Santa Cruz (sc-66048)
GFP	1:1000 (WB)	Roche (11814460001)
Ubiquitin	1:1000 (WB)	Cell Signaling Technology (3933S)
HA (HRP conjugate)	1:1000 (WB)	Thermo (26183-HRP)
L. pneumophila	1:2000 (opsonization)	Thermo (PA1-7227)
Goat anti-Rabbit IgG (H+L) Highly Cross-Adsorbed Secondary Antibody (Alexa Fluor 633)	1:500 (IF)	Life Technologies (a21071)
Goat anti-Mouse IgG (H+L) Highly Cross-Adsorbed Secondary Antibody (Alexa Fluor 488)	1:500 (IF)	Life Technologies (a11029)
Goat Anti-Mouse IgG (H+L) HRP Conjugate	1:5000 (WB)	Life Technologies (A16066)
Goat Anti-Rabbit IgG (H+L) HRP Conjugate	1:5000 (WB)	Life Technologies (A16096)
Mouse Anti rabbit IgG (Conformation Specific) - HRP conjugate	1:2000 (WB) - used for ubiquitin immunoblots to avoid detection of opsonization antibody	Cell Signaling Technology (5127S)
Kits		
Signal-Seeker™ Ubiquitination Detection Kit	Cytoskeleton, Inc.	Cat.# BK161
Software and algorithms		
Name	**Source**	**Link**
MaxQuant	(Cox *et al.*, 2014)	https://www.maxquant.org
artMS Bioconductor package (v 0.9)	(Jimenez-Morales *et al.*, 2019)	https://bioconductor.org/packages/release/bioc/html/artMS.html
factoextra R package	(Jimenez-Morales *et al.*, 2023)	https://zenodo.org/record/8093247
Metascape	(Zhou *et al.*, 2019)	https://metascape.org
DeepVenn	(Hulsen, 2022)	https://www.deepvenn.com
Jalview	(Waterhouse *et al.*, 2009)	https://www.jalview.org
Fiji	(Schindelin *et al.*, 2012)	https://fiji.sc
Prism	Graphpad	https://www.graphpad.com
ggplot2 (R package for generating plots)		https://ggplot2.tidyverse.org
UCSF ChimeraX	(Pettersen *et al.*, 2021)	https://www.cgl.ucsf.edu/chimerax/
Deposited data		
Raw data from mass spectrometry	ProteomeXchange Consortium (http://proteomecentral.proteomexchange.org) via PRIDE partner repository	PXD019217

TABLE 1: Key resources. Continued

DATA AVAILABILITY

The mass spectrometry data files have been deposited to the ProteomeXchange Consortium (http://proteomecentral.proteomexchange.org) via the PRIDE partner repository with the dataset identifier PXD019217 (Vizcaíno *et al.*, 2016).

REFERENCES

Aktories K, Schmidt G (2014). General Features, Signaling. In: Ras Superfamily Small G Proteins: Biology and Mechanisms 1, ed. Wittinghofer A, Vienna, Austria: Springer Vienna, 65–97.

Anand IS, Choi W, Isberg RR (2020). Components of the endocytic and recycling trafficking pathways interfere with the integrity of the Legionella-containing vacuole. Cell Microbiol 22, e13151.

Baker R, Lewis SM, Sasaki AT, Wilkerson EM, Locasale JW, Cantley LC, Kuhlman B, Dohlman HG, Campbell SL (2013). Site-specific monoubiquitination activates Ras by impeding GTPase-activating protein function. Nat Struct Mol Biol 20, 46–52.

Berger KH, Isberg RR (1993). Two distinct defects in intracellular growth complemented by a single genetic locus in Legionella pneumophila. Mol Microbiol 7, 7–19.

Berger KH, Merriam JJ, Isberg RR (1994). Altered intracellular targeting properties associated with mutations in the Legionella pneumophila dotA gene. Mol Microbiol 14, 809–822.

Best A, Kwaik YA (2018). Evolution of the arsenal of Legionella pneumophila effectors to modulate protist hosts. mBio 9, e01313–18.

Bhogaraju S, Kalayil S, Liu Y, Bonn F, Colby T, Matic I, Dikic I (2016). Phosphoribosylation of ubiquitin promotes serine ubiquitination and impairs conventional ubiquitination. Cell 167, 1636–1649.e13.

Black MH, Osinski A, Gradowski M, Servage KA, Pawłowski K, Tomchick DR, Tagliabracci VS (2019). Bacterial pseudokinase catalyzes protein polyglutamylation to inhibit the SidE-family ubiquitin ligases. Science 364, 787–792.

Budzik JM, Swaney DL, Jimenez-Morales D, Johnson JR, Garelis NE, Repasy T, Roberts AW, Popov LM, Parry TJ, Pratt D, et al. (2020). Dynamic post-translational modification profiling of M. tuberculosis-infected primary macrophages. eLife 9, e51461.

Chen P-I, Kong C, Su X, Stahl PD (2009). Rab5 isoforms differentially regulate the trafficking and degradation of epidermal growth factor receptors*. J Biol Chem 284, 30328–30338.

Chen P-I, Schauer K, Kong C, Harding AR, Goud B, Stahl PD (2014). Rab5 isoforms orchestrate a "division of labor" in the endocytic network; Rab5C modulates Rac-mediated cell motility. PLoS One 9, e90384.

Cherfils J, Zeghouf M (2013). Regulation of small GTPases by GEFs, GAPs, and GDIs. Physiol Rev 93, 269–309.

Choi M, Chang C-Y, Clough T, Broudy D, Killeen T, MacLean B, Vitek O (2014). MSstats: an R package for statistical analysis of quantitative mass spectrometry-based proteomic experiments. Bioinformatics 30, 2524–2526.

Clemens DL, Lee B-Y, Horwitz MA (2000a). Deviant expression of Rab5 on phagosomes containing the intracellular pathogens Mycobacterium tuberculosis and Legionella pneumophila is associated with altered phagosomal fate. Infect Immun 68, 2671–2684.

Clemens DL, Lee B-Y, Horwitz MA (2000b). Mycobacterium tuberculosis and Legionella pneumophila phagosomes exhibit arrested maturation despite acquisition of Rab7. Infect Immun 68, 5154–5166.

Cox J, Hein MY, Luber CA, Paron I, Nagaraj N, Mann M (2014). Accurate proteome-wide label-free quantification by delayed normalization and maximal peptide ratio extraction. Termed MaxLFQ*. Mol Cell Proteomics 13, 2513–2526.

Derré I, Isberg RR (2004). Legionella pneumophila replication vacuole formation involves rapid recruitment of proteins of the early secretory system. Infect Immun 72, 3048–3053.

Dewhurst HM, Choudhury S, Torres MP (2015). Structural analysis of PTM hotspots (SAPH-ire) – a quantitative informatics method enabling the discovery of novel regulatory elements in protein families* [S]. Mol Cell Proteomics 14, 2285–2297.

Dohlman HG, Campbell SL (2019). Regulation of large and small G proteins by ubiquitination. J Biol Chem 294, 18613–18623.

Dong N, Niu M, Hu L, Yao Q, Zhou R, Shao F (2016). Modulation of membrane phosphoinositide dynamics by the phosphatidylinositide 4-kinase activity of the Legionella LepB effector. Nat Microbiol 2, 16236.

Dorer MS, Kirton D, Bader JS, Isberg RR (2006). RNA Interference analysis of Legionella in Drosophila cells: exploitation of early secretory apparatus dynamics. PLoS Pathog 2, e34.

Duncan ED, Han K-J, Trout MA, Prekeris R (2022). Ubiquitylation by Rab40b/Cul5 regulates Rap2 localization and activity during cell migration. J Cell Biol 221, e202107114.

Dwingelo JV, Chung IYW, Price CT, Li L, Jones S, Cygler M, Kwaik YA (2019). Interaction of the Ankyrin H core effector of Legionella with the host LARP7 component of the 7SK snRNP complex. mBio 10, e01942–19.

Emmerich CH, Cohen P (2015). Optimising methods for the preservation, capture and identification of ubiquitin chains and ubiquitylated proteins by immunoblotting. Biochem Bioph Res Co 466, 1–14.

Fajardo M, Schleicher M, Noegel A, Bozzaro S, Killinger S, Heuner K, Hacker J, Steinert M (2004). Calnexin, calreticulin and cytoskeleton-associated proteins modulate uptake and growth of Legionella pneumophila in Dictyostelium discoideum. Microbiology+ 150, 2825–2835.

Fiskin E, Bionda T, Dikic I, Behrends C (2016). Global analysis of host and bacterial ubiquitinome in response to Salmonella Typhimurium infection. Mol Cell 62, 967–981.

Gaspar AH, Machner MP (2014). VipD is a Rab5-activated phospholipase A1 that protects Legionella pneumophila from endosomal fusion. Proc Natl Acad Sci USA 111, 4560–4565.

Gomez-Valero L, Buchrieser C (2019). Intracellular parasitism, the driving force of evolution of Legionella pneumophila and the genus Legionella. Microbes Infect 21, 230–236.

Goody RS, Müller MP, Wu Y-W (2017). Mechanisms of action of Rab proteins, key regulators of intracellular vesicular transport. Biol Chem 398, 565–575.

Hardiman CA, Roy CR (2014). AMPylation is critical for Rab1 localization to vacuoles containing Legionella pneumophila. mBio 5, e01035–13.

Hoffmann C, Finsel I, Otto A, Pfaffinger G, Rothmeier E, Hecker M, Becher D, Hilbi H (2014). Functional analysis of novel Rab GTPases identified in the proteome of purified Legionella-containing vacuoles from macrophages. Cell Microbiol 16, 1034–1052.

Homma Y, Hiragi S, Fukuda M (2021). Rab family of small GTPases: an updated view on their regulation and functions. Febs J 288, 36–55.

Horenkamp FA, Mukherjee S, Alix E, Schauder CM, Hubber AM, Roy CR, Reinisch KM (2014). Legionella pneumophila subversion of host vesicular transport by SidC effector proteins. Traffic 15, 488–499.

Hsu F, Luo X, Qiu J, Teng Y-B, Jin J, Smolka MB, Luo Z-Q, Mao Y (2014). The Legionella effector SidC defines a unique family of ubiquitin ligases important for bacterial phagosomal remodeling. Proc National Acad Sci 111, 10538–10543.

Hubber A, Roy CR (2010). Modulation of host cell function by Legionella pneumophila type IV effectors. Annu Rev Cell Dev Bi 26, 261–283.

Hulsen T (2022). DeepVenn – a web application for the creation of area-proportional Venn diagrams using the deep learning framework Tensorflow. js. arXiv, https://doi.org/10.48550/arXiv.2210.04597.

Ingmundson A, Delprato A, Lambright DG, Roy CR (2007). Legionella pneumophila proteins that regulate Rab1 membrane cycling. Nature 450, 365–369.

Ivanov SS, Roy CR (2009). Modulation of ubiquitin dynamics and suppression of DALIS formation by the Legionella pneumophila Dot/Icm system. Cell Microbiol 11, 261–278.

Ivanov SS, Roy CR (2013). Pathogen signatures activate a ubiquitination pathway that modulates the function of the metabolic checkpoint kinase mTOR. Nat Immunol 14, 1219–1228.

Jeng EE, Bhadkamkar V, Ibe NU, Gause H, Jiang L, Chan J, Jian R, Jimenez-Morales D, Stevenson E, Krogan NJ, et al. (2019). Systematic identification of host cell regulators of legionella pneumophila pathogenesis using a Genome-wide CRISPR screen. Cell Host Microbe 26, 551–563.

Jeong KC, Sexton JA, Vogel JP (2015). Spatiotemporal regulation of a Legionella pneumophila T4SS substrate by the Metaeffector SidJ. PLoS Pathog 11, e1004695.

Jimenez-Morales D, Campos AR, Dollen JV (2019). artMS: analytical R tools for mass spectrometry. Bioconductor.

Jimenez-Morales D, Turaga N, Dollen JV, Bpolacco, Campos A, Zhouyuan A, Obenchain V, King E (2023). biodavidjm/artMS: artMS for Zenodo, Zenodo. https://zenodo.org/records/8093247.

Kagan JC, Roy CR (2002). Legionella phagosomes intercept vesicular traffic from endoplasmic reticulum exit sites. Nat Cell Biol 4, 945–954.

Kagan JC, Stein M-P, Pypaert M, Roy CR (2004). Legionella subvert the functions of Rab1 and Sec22b to create a replicative organelle. J Exp Medicine 199, 1201–1211.

Kawabata M, Matsuo H, Koito T, Murata M, Kubori T, Nagai H, Tagaya M, Arasaki K (2021). Legionella hijacks the host Golgi-to-ER retrograde pathway for the association of Legionella-containing vacuole with the ER. PLoS Pathog 17, e1009437.

Kholmanskikh S, Singh S, Ross ME (2022). Activation of RhoC by regulatory ubiquitination is mediated by LNX1 and suppressed by LIS1. Sci Rep 12, 16493.

Kim S, Isberg RR (2023). The Sde Phosphoribosyl-linked ubiquitin transferases protect the Legionella pneumophila vacuole from degradation by the host. Proc Natl Acad Sci 120, e2303942120.

Kim W, Bennett EJ, Huttlin EL, Guo A, Li J, Possemato A, Sowa ME, Rad R, Rush J, Comb MJ, et al. (2011). Systematic and quantitative assessment of the ubiquitin-modified proteome. Mol Cell 44, 325–340.

Komander D, Rape M (2012). The ubiquitin code. Annu Rev Biochem 81, 203–229.

Lachance V, Degrandmaison J, Marois S, Robitaille M, Génier S, Nadeau S, Angers S, Parent J-L (2013). Ubiquitylation and activation of a Rab GTPase is promoted by a β2AR–HACE1 complex. J Cell Sci 127, 111–123.

Langemeyer L, Fröhlich F, Ungermann C (2018). Rab GTPase function in endosome and lysosome biogenesis. Trends Cell Biol 28, 957–970.

Lei Z, Wang J, Zhang L, Liu CH (2021). Ubiquitination-dependent regulation of small GTPases in membrane trafficking: from cell biology to human diseases. Front Cell Dev Biol 9, 688352.

Levin RS, Hertz NT, Burlingame AL, Shokat KM, Mukherjee S (2016). Innate immunity kinase TAK1 phosphorylates Rab1 on a hotspot for posttranslational modifications by host and pathogen. Proc Natl Acad Sci USA 113, E4776–E4783.

Li X, Anderson DE, Chang Y-Y, Jarnik M, Machner MP (2022). VpdC is a ubiquitin-activated phospholipase effector that regulates Legionella vacuole expansion during infection. Proc Natl Acad Sci USA 119, e2209149119.

Liu S, Jiwei L, Zhen X, Qiu J, Ouyang S, Luo Z-Q (2020). Interplay between bacterial deubiquitinase and ubiquitin E3 ligase regulates ubiquitin dynamics on Legionella phagosomes. eLife 9, e58114.

Lockwood DC, Amin H, Costa TRD, Schroeder GN (2022). The Legionella pneumophila Dot/Icm type IV secretion system and its effectors. Microbiol 168, 001187.

Luo J, Wang L, Song L, Luo Z-Q (2021). Exploitation of the host ubiquitin system: means by Legionella pneumophila. Front Microbiol 12, 790442.

Luo Z-Q, Isberg RR (2004). Multiple substrates of the Legionella pneumophila Dot/Icm system identified by interbacterial protein transfer. P Natl Acad Sci Usa 101, 841–846.

Machner MP, Isberg RR (2006). Targeting of host Rab GTPase function by the intravacuolar pathogen Legionella pneumophila. Dev Cell 11, 47–56.

Mertins P, Qiao JW, Patel J, Udeshi ND, Clauser KR, Mani DR, Burgess MW, Gillette MA, Jaffe JD, Carr SA (2013). Integrated proteomic analysis of post-translational modifications by serial enrichment. Nat Methods 10, 634–637.

Moss SM, Taylor IR, Ruggero D, Gestwicki JE, Shokat KM, Mukherjee S (2019). A Legionella pneumophila kinase phosphorylates the Hsp70 chaperone family to inhibit eukaryotic protein synthesis. Cell Host Microbe 25, 454–462.

Mukherjee S, Liu X, Arasaki K, McDonough J, Galán JE, Roy CR (2011). Modulation of Rab GTPase function by a protein phosphocholine transferase. Nature 477, 103–106.

Müller MP, Goody RS (2017). Molecular control of Rab activity by GEFs, GAPs and GDI. Small Gtpases 9, 5–21.

Müller MP, Peters H, Blümer J, Blankenfeldt W, Goody RS, Itzen A (2010). The Legionella effector protein DrrA AMPylates the membrane traffic regulator Rab1b. Science 329, 946–949.

Murata T, Delprato A, Ingmundson A, Toomre DK, Lambright DG, Roy CR (2006). The Legionella pneumophila effector protein DrrA is a Rab1 guanine nucleotide-exchange factor. Nat Cell Biol 8, 971–977.

Nagai H, Kagan JC, Zhu X, Kahn RA, Roy CR (2002). A bacterial guanine nucleotide exchange factor activates ARF on Legionella Phagosomes. Science 295, 679–682.

Neunuebel MR, Mohammadi S, Jarnik M, Machner MP (2012). Legionella pneumophila LidA affects nucleotide binding and activity of the host GTPase Rab1. J Bacteriol 194, 1389–1400.

Oliva G, Sahr T, Buchrieser C (2018). The life cycle of L. pneumophila: cellular differentiation is linked to virulence and metabolism. Front Cell Infect Mi 8, 3.

Ong SY, Schuelein R, Wibawa RR, Thomas DW, Handoko Y, Freytag S, Bahlo M, Simpson KJ, Hartland EL (2021). Genome-wide genetic screen identifies host ubiquitination as important for Legionella pneumophila Dot/Icm effector translocation. Cell Microbiol 23, e13368.

Osaka N, Hirota Y, Ito D, Ikeda Y, Kamata R, Fujii Y, Chirasani VR, Campbell SL, Takeuchi K, Senda T, Sasaki AT (2021). Divergent mechanisms activating RAS and small GTPases through post-translational modification. Front Mol Biosci 8, 707439.

Peng H, Yang J, Li G, You Q, Han W, Li T, Gao D, Xie X, Lee BH, Du J, et al. (2017). Ubiquitylation of p62/sequestosome1 activates its autophagy receptor function and controls selective autophagy upon ubiquitin stress. Cell Res 27, 657–674.

Pettersen EF, Goddard TD, Huang CC, Meng EC, Couch GS, Croll TI, Morris JH, Ferrin TE (2021). UCSF ChimeraX: structure visualization for researchers, educators, and developers. Protein Sci 30, 70–82.

Price CTD, Al-Quadan T, Santic M, Rosenshine I, Kwaik YA (2011). Host proteasomal degradation generates amino acids essential for intracellular bacterial growth. Science 334, 1553–1557.

Qiu J, Luo Z-Q (2017). Legionella and Coxiella effectors: strength in diversity and activity. Nat Rev Micro 15, 591–605.

Qiu J, Sheedlo MJ, Yu K, Tan Y, Nakayasu ES, Das C, Liu X, Luo Z-Q (2016). Ubiquitination independent of E1 and E2 enzymes by bacterial effectors. Nature 533, 120–124.

Ragaz C, Pietsch H, Urwyler S, Tiaden A, Weber SS, Hilbi H (2008). The Legionella pneumophila phosphatidylinositol-4 phosphate-binding type IV substrate SidC recruits endoplasmic reticulum vesicles to a replication-permissive vacuole. Cell Microbiol 10, 2416–2433.

Rolando M, Sanulli S, Rusniok C, Gomez-Valero L, Bertholet C, Sahr T, Margueron R, Buchrieser C (2013). Legionella pneumophila effector RomA uniquely modifies host chromatin to repress gene expression and promote intracellular bacterial replication. Cell Host Microbe 13, 395–405.

Rothmeier E, Pfaffinger G, Hoffmann C, Harrison CF, Grabmayr H, Repnik U, Hannemann M, Wölke S, Bausch A, Griffiths G, et al. (2013). Activation of Ran GTPase by a Legionella effector promotes microtubule polymerization, pathogen vacuole motility and infection. PLoS Pathog 9, e1003598.

Roy CR, Berger KH, Isberg RR (1998). Legionella pneumophila DotA protein is required for early phagosome trafficking decisions that occur within minutes of bacterial uptake. Mol Microbiol 28, 663–674.

Sapmaz A, Berlin I, Bos E, Wijdeven RH, Janssen H, Konietzny R, Akkermans JJ, Erson-Bensan AE, Koning RI, Kessler BM, et al. (2019). USP32 regulates late endosomal transport and recycling through deubiquitylation of Rab7. Nat Commun 10, 1454.

Sasaki AT, Carracedo A, Locasale JW, Anastasiou D, Takeuchi K, Kahoud ER, Haviv S, Asara JM, Pandolfi PP, Cantley LC (2011). Ubiquitination of K-Ras enhances activation and facilitates binding to select downstream effectors. Sci Signal 4, ra13.

Schator D, Mondino S, Berthelet J, Silvestre CD, Assaya MB, Rusniok C, Rodrigues-Lima F, Wehenkel A, Buchrieser C, Rolando M (2023). Legionella para-effectors target chromatin and promote bacterial replication. Nat Commun 14, 2154.

Schindelin J, Arganda-Carreras I, Frise E, Kaynig V, Longair M, Pietzsch T, Preibisch S, Rueden C, Saalfeld S, Schmid B, et al. (2012). Fiji: an open-source platform for biological-image analysis. Nat Methods 9, 676–682.

Schmölders J, Manske C, Otto A, Hoffmann C, Steiner B, Welin A, Becher D, Hilbi H (2017). Comparative proteomics of purified pathogen vacuoles correlates intracellular replication of Legionella pneumophila with the small GTPase Ras-related protein 1 (Rap1)*. Mol Cell Proteomics 16, 622–641.

Schoebel S, Cichy AL, Goody RS, Itzen A (2011). Protein LidA from Legionella is a Rab GTPase supereffector. Proc Natl Acad Sci USA 108, 17945–17950.

Schuelein R, Spencer H, Dagley LF, Li P, Luo L, Stow JL, Abraham G, Naderer T, Gomez-Valero L, Buchrieser C, et al. (2018). Targeting of RNA polymerase II by a nuclear Legionella pneumophila Dot/Icm effector SnpL. Cell Microbiol 20, e12852.

Shin D, Mukherjee R, Liu Y, Gonzalez A, Bonn F, Liu Y, Rogov VV, Heinz M, Stolz A, Hummer G, et al. (2020). Regulation of phosphoribosyl-linked serine ubiquitination by deubiquitinases DupA and DupB. Mol Cell 77, 164–179.e6.

Shin D, Na W, Lee J-H, Kim G, Baek J, Park SH, Choi CY, Lee S (2017). Site-specific monoubiquitination downregulates Rab5 by disrupting effector binding and guanine nucleotide conversion. eLife 6, e29154.

Shin HW, Hayashi M, Christoforidis S, Lacas-Gervais S, Hoepfner S, Wenk MR, Modregger J, Uttenweiler-Joseph S, Wilm M, Nystuen A, *et al.* (2005). An enzymatic cascade of Rab5 effectors regulates phosphoinositide turnover in the endocytic pathway. J Cell Biol 170, 607–618.

Simon S, Wagner MA, Rothmeier E, Müller-Taubenberger A, Hilbi H (2014). Icm/Dot-dependent inhibition of phagocyte migration by Legionella is antagonized by a translocated Ran GTPase activator. Cell Microbiol 16, 977–992.

Simonsen A, Lippe R, Christoforidis S, Gaullier J-M, Brech A, Callaghan J, Toh B-H, Murphy C, Zerial M, Stenmark H (1998). EEA1 links PI(3)K function to Rab5 regulation of endosome fusion. Nature 394, 494–498.

Sohn Y-S, Shin H-C, Park WS, Ge J, Kim C-H, Lee BL, Heo WD, Jung JU, Rigden DJ, Oh B-H (2015). Lpg0393 of Legionella pneumophila Is a guanine-nucleotide exchange factor for Rab5, Rab21 and Rab22. PLoS One 10, e0118683.

Steger M, Tonelli F, Ito G, Davies P, Trost M, Vetter M, Wachter S, Lorentzen E, Duddy G, Wilson S, *et al.* (2016). Phosphoproteomics reveals that Parkinson's disease kinase LRRK2 regulates a subset of Rab GTPases. eLife 5, e12813.

Steiner B, Weber S, Hilbi H (2018). Formation of the Legionella-containing vacuole: phosphoinositide conversion, GTPase modulation and ER dynamics. Int J Med Microbiol 308, 49–57.

Steklov M, Pandolfi S, Baietti MF, Batiuk A, Carai P, Najm P, Zhang M, Jang H, Renzi F, Cai Y, *et al.* (2018). Mutations in LZTR1 drive human disease by dysregulating RAS ubiquitination. Science 362, 1177–1182.

Swart AL, Steiner B, Gomez-Valero L, Schütz S, Hannemann M, Janning P, Irminger M, Rothmeier E, Buchrieser C, Itzen A, *et al.* (2020). Divergent evolution of Legionella RCC1 repeat effectors defines the range of Ran GTPase cycle targets. mBio 11, e00405–20.

Tan Y, Arnold RJ, Luo Z-Q (2011). Legionella pneumophila regulates the small GTPase Rab1 activity by reversible phosphorylcholination. Proc Natl Acad Sci USA 108, 21212–21217.

Torres M (2016). Chapter Two - heterotrimeric G protein ubiquitination as a regulator of G protein signaling. Prog Mol Biol Transl 141, 57–83.

Tran CS, Eran Y, Ruch TR, Bryant DM, Datta A, Brakeman P, Kierbel A, Wittmann T, Metzger RJ, Mostov KE, Engel JN, *et al.* (2014). Host cell polarity proteins participate in innate immunity to Pseudomonas aeruginosa infection. Cell Host Microbe 15, 636–643.

Treacy-Abarca S, Mukherjee S (2015). Legionella suppresses the host unfolded protein response via multiple mechanisms. Nat Commun 6, 7887.

Vizcaíno JA, Csordas A, del-Toro N, Dianes JA, Griss J, Lavidas I, Mayer G, Perez-Riverol Y, Reisinger F, Ternent T, *et al.* (2016). 2016 update of the PRIDE database and its related tools. Nucleic Acids Res 44, D447–D456.

Waterhouse AM, Procter JB, Martin DMA, Clamp M, Barton GJ (2009). Jalview Version 2—a multiple sequence alignment editor and analysis workbench. Bioinformatics 25, 1189–1191.

Webb-Robertson BJM, Wiberg HK, Matzke MM, Brown JN, Wang J, McDermott JE, Smith RD, Rodland KD, Metz TO, Pounds JG, Waters KM (2015). Review, evaluation, and discussion of the challenges of missing value imputation for mass spectrometry-based label-free global proteomics. J Proteome Res 14, 1993–2001.

Weber SS, Ragaz C, Reus K, Nyfeler Y, Hilbi H (2006). Legionella pneumophila exploits PI(4)P to anchor secreted effector proteins to the replicative vacuole. PLoS Pathog 2, e46.

Xu G, Paige JS, Jaffrey SR (2010). Global analysis of lysine ubiquitination by ubiquitin remnant immunoaffinity profiling. Nat Biotechnol 28, 868–873.

Yau R, Rape M (2016). The increasing complexity of the ubiquitin code. Nat Cell Biol 18, 579–586.

Zhou Y, Zhou B, Pache L, Chang M, Khodabakhshi AH, Tanaseichuk O, Benner C, Chanda SK (2019). Metascape provides a biologist-oriented resource for the analysis of systems-level datasets. Nat Commun 10, 1523.